Microphysical Properties of Supercooled Large Droplet Conditions in North America and Europe

Johannes Lucke,* Tina Jurkat-Witschas,† Deniz Menekay,‡ and Christiane Voigt§
German Aerospace Center, 82234 Wessling, Germany
Ben C. Bernstein¶
Leading Edge Atmospherics, Longmont, Colorado 80504
Olivier Jaron**
CNRM, 31100 Toulouse, France
Aurelien Bourdon††
CNRS, 31270 Cugnaux, France
and
Gabriel Silva Garcia‡‡
Embraer S.A., São José dos Campos, SP 12227-000, Brazil

https://doi.org/10.2514/1.D0469

Supercooled large droplet (SLD) icing conditions threaten aviation safety. Two flight campaigns in SLD conditions were performed in February–March 2023 in the Great Lakes region and in April 2023 over France as part of the EU project SENS4ICE. This provides the opportunity to contrast and compare the observations of SLDs between these two locations and months. We present the altitudes, temperatures, number concentrations, liquid water contents, and cumulative mass distributions of the SLD conditions. During the North American flight campaign, SLD conditions were observed mostly in thick stratus clouds, and droplet size distributions were bimodal with an average median volume diameter (MVD) of 23 μm. Due to warmer ground temperatures in April, icing conditions during the European campaign occurred at higher altitudes; hence, predominantly midlevel clouds were sampled. The average MVD of SLD conditions was 45 μm. Our study suggests that the maritime origin of the European air masses, their likely low levels of pollution, and the associated low number of cloud condensation nuclei facilitated the formation of these SLD conditions with relatively large MVDs. The presented dataset can serve for model comparisons, process-oriented studies of icing conditions, and the validation of airborne sensors developed in the Sensors and Certifiable Hybrid Architectures for Safer Aviation in Icing Environment (SENS4ICE) project.

Nomenclature

CCN	=	cloud condensation nucleus
CDP	=	cloud droplet probe
CER	=	circulation Essais et Réception
CIP	=	cloud imaging probe
c	=	constant that relates the shadowing level with the depth of field
D	=	diameter
DLR	=	German Aerospace Center
DOF	=	depth of field
DSD	=	droplet size distribution
FZDZ	=	freezing drizzle
HSI	=	high-speed imaging probe
ICD	=	ice crystal detector
INP	=	ice nucleating particle
LAS	=	large aspherical particles
LWC	=	liquid water content
MVD	=	median volume diameter
N	=	number concentration
NWP	=	numerical weather prediction
OAP	=	optical array probe
OF	=	observational flight
PIP	=	precipitation imaging probe
PSD	=	particle size distribution
SEA	=	Science Engineering Associates, Inc.
SENS4ICE	=	SENSors and certifiable hybrid architectures for safer aviation in ICing Environment
SLD	=	supercooled large droplet
TF	=	test flight
TWC	=	total water content
VD_n	=	diameter specifying the nth percentile of the cumulative mass distribution
χ	=	parameter that corresponds to a shadowing level of an optical array
λ	=	wavelength

Subscript

HW	=	hotwire

Presented as Paper 2024-3526 at the AIAA Aviation 2024 Forum, Las Vegas, NV, July 29–August 2, 2024; received 1 August 2024; accepted for publication 16 April 2025; published online Open Access 17 July 2025.

*Researcher, Institute of Atmospheric Physics, Münchener Straße 20, Germany; also Ph.D. Student, Delft University of Technology, Faculty of Aerospace Engineering, Delft 2629, The Netherlands; currently Rail Tec Arsenal, Paukerwerkstraße 3, 1210 Vienna, Austria; johanneslucke@gmail.com. Member AIAA (Corresponding Author).

†Project Manager, Researcher, Institute of Atmospheric Physics, Münchener Straße 20, Germany.

‡Researcher, Institute of Atmospheric Physics, Münchener Straße 20, 82234 Wessling, Germany; also Ph.D. Student, Technical University of Munich, Chair of Astronomical and Physical Geodesy, Arcisstraße 21, Munich, Germany.

§Head of Department Cloud Physics, Institute of Atmospheric Physics, Münchener Straße 20, Germany; also Professor, Institute of Atmospheric Physics, University of Mainz, Mainz 55881, Germany.

¶Meteorological Consultant, 2125 Ridgeview Way, Longmont, CO 80504, USA. Member AIAA.

**Engineer, Centre de Météorologie Spatiale, Météo-France, Avenue de Lorraine, 22300 Lannion, France.

††Research Engineer, SAFIRE (CNRS / Météo-France / CNES), Aéroport Toulouse-Francazal, 31270 Cugnaux, France.

‡‡Product Development Engineer, Ice Protection Systems, Av. Brg. Faria Lima, 2170, São José dos Campos, SP 12227-000, Brazil.

I. Introduction

SUPERCOOLED large droplets (SLDs) represent a hazard to aviation [1–3]. SLDs are defined as supercooled drops with a diameter larger than 100 μm [4]. Due to their large inertia, these drops may strike aircraft surfaces that are not covered by the ice protection system. Before the fatal accident of American Eagle flight 4184 in 1994 near Roselawn, Indiana [5,6], the aviation regulations for flight in icing conditions only required aircraft manufacturers to prove that their aircraft could fly safely in the icing conditions specified in Appendix C to Part 25 of American and European regulations. These icing conditions (which are often referred to as Appendix C conditions) only considered droplet size distributions with median volume diameters (MVDs) up to 50 μm; hence, SLDs were not explicitly included.

The Roselawn accident prompted various research activities, which eventually led to the development of a new standard for flight in SLD conditions [7], which was added to the aviation regulations as Appendix O [8,9]. SLD icing conditions are therefore referred to as Appendix O conditions.

Appendix O conditions form either through the supercooled warm rain process, where cloud droplets first grow from the vapor phase and then coalesce until they attain the size of SLDs, or from frozen particles that melt during passage through a warm layer and subsequently supercool in a cold layer [6]. The first process produces predominantly freezing drizzle (FZDZ), with SLDs generally smaller than 500 μm. The second process generally produces freezing rain (FZRA), where SLD diameters can be well above 500 μm.

Apart from describing microphysical characteristics, Appendix O also sets standards for the certification of new aircraft. New aircraft are required to detect the presence of Appendix O conditions unless they can operate safely in all Appendix O conditions. The SENS4ICE project [10–12] therefore investigated sensor designs [13] and an indirect ice detection technology [14,15] that provide information on the presence of icing and Appendix O conditions. Seven new sensor designs were flight tested during two dedicated flight campaigns with research aircraft over the United States and France. In addition to the newly developed sensors, the research aircraft carried established scientific airborne instrumentation to accurately characterize the icing conditions and to provide a reference for the new sensors [16]. The data from these scientific instruments and the findings on the characteristics of icing conditions are the focus of this work. For safety reasons, the flight campaigns targeted only FZDZ conditions and not FZRA.

While Appendix O has been established, it has not been widely applied in aircraft certification yet. Aircraft types certified before the introduction of Appendix O do not need to show compliance, meaning that such aircraft are still put into service and consequently will fly for decades. Recent incidents demonstrate that SLDs still pose a hazard [17–21]. An improved understanding of the formation, occurrence, and severity of SLD conditions is therefore important.

There is a wealth of SLD flight data from the North American continent [4,22–25], and the Great Lakes region, where the North American SENS4ICE campaign took place, is known as a hotspot for SLD conditions [26]. On the other hand, less data exist from Europe. A measurement campaign targeting SLD conditions over Southern Germany is described by Hauf and Schröder [27], while icing events over Spain were analyzed by Fernández-González et al. [28] and Bolgiani et al. [29]. The SENS4ICE measurements over France add a new perspective to the research on icing conditions in Europe. They were collected during springtime, often in midlevel clouds and many times in clean, maritime air masses. The Pyrenees contributed to lifting and blocking effects on several occasions.

This work evaluates the liquid water contents (LWCs), total water contents (TWCs), number concentrations, and size distributions of the Appendix O and Appendix C conditions encountered in the two flight campaigns and thereby increases the amount of data available on icing conditions. The different geographical locations where data were collected also allow us to investigate some of the factors that influence the number concentrations and size distributions of SLD conditions.

This work is structured as follows: First, an overview of the two flight campaigns is given. Then, the scientific instrumentation on the aircraft is described. This is followed by a section that details the data evaluation. From the evaluated data, we derive the macro- and microphysical properties of the icing conditions in the two flight campaigns. Finally, we discuss the central observations and the implications for aircraft certification and operation as well as further research needs.

II. SENS4ICE Flight Campaigns

A. North American Flight Campaign

The North American flight campaign took place in February and March 2023 and was based out of Alton, Illinois (KALN). The research aircraft was a Phenom 300 business jet, owned and operated by Embraer S.A. Eight measurement flights from this campaign are evaluated in this work, which are listed in Table 1 and shown in the map in Fig. 1. Flight 1478 and Flight 1482 consisted of two flight legs that are not displayed separately because the data recording was not interrupted during the refueling stop. Over the course of the North American program, a total of 4 h and 23 min were spent in icing conditions, 50 min of which were in Appendix O icing conditions. The flights generally sampled north of Alton, with only Flight 1482 heading almost directly to the east. Several flights passed over or close to Lake Michigan or Lake Erie. A detailed meteorological analysis of the flights has been compiled by Bernstein [30].

The sampling strategy for the North American campaign followed a well-defined procedure to ensure safety. Before the campaign, a reference exposure time in Appendix O was defined to provide adequate sampling time for the sensor demonstration while keeping high safety margins regarding ice accretion. The aircraft entered the clouds from the top and then descended deeper into the clouds. The icing conditions were monitored and compared to the reference Appendix O conditions. The exposure time was reduced (increased) if icing conditions were more (less) severe than the reference conditions. The aircraft always exited the clouds through the cloud top and remained outside of icing conditions until clear of ice. The aircraft performed well in all icing conditions. Due to the sampling strategy, the data from the North American campaign are representative of FZDZ conditions near the cloud top but may not represent conditions deeper within the clouds. The average speed of the Phenom during sampling was 90 m s^{-1}, significantly lower than the normal cruise speed.

The North American campaign sampled mostly in thick stratus cloud decks. Figure 2 shows cloud bottom and cloud top altitudes as well as the resulting cloud depth. The cloud depths are based on data from profiles through or into the cloud. These profiles either occurred after takeoff and before landing or during sampling, when the plane descended into the cloud deck. In the second case, the

Table 1 Flights of the North American SENS4ICE campaign

Flight	Date	Flight time (UTC)	Time in icing conditions [mm:ss]	Time in Appendix O conditions [mm:ss]	Airmass origin
F1475-1	23/02/23	11:43–14:29	20:33	09:14	Continental
F1475-2	23/02/23	17:18–18:33	19:56	00:00	Continental
F1476	25/02/23	11:38–13:43	38:53	22:59	Continental
F1477-1	01/03/23	11:38–13:48	31:09	04:15	Continental
F1477-2	01/03/23	16:56–18:34	14:52	07:31	Continental
F1478	06/03/23	11:46–14:18	43:36	04:33	Continental
F1481	09/03/23	12:01–13:13	16:07	02:44	Continental
F1482	10/03/23	12:08–17:40	78:43	00:00	Continental

The flight tracks are shown color-coded in Fig. 1. The implications of the airmass origin are discussed in Sec. V.B.

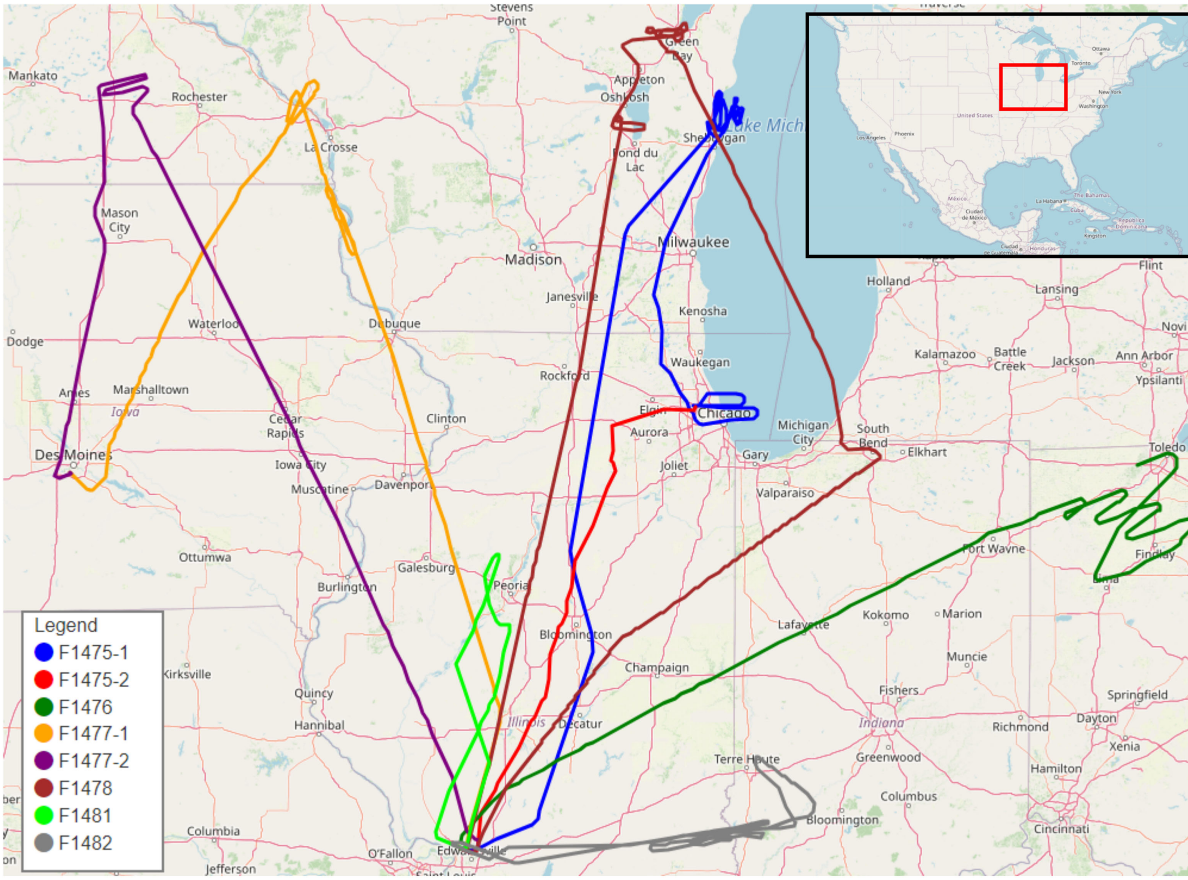

Fig. 1 Flights conducted within the North American SENS4ICE campaign. Map from OpenStreetMap. The flights were based out of Alton, Illinois (KALN).

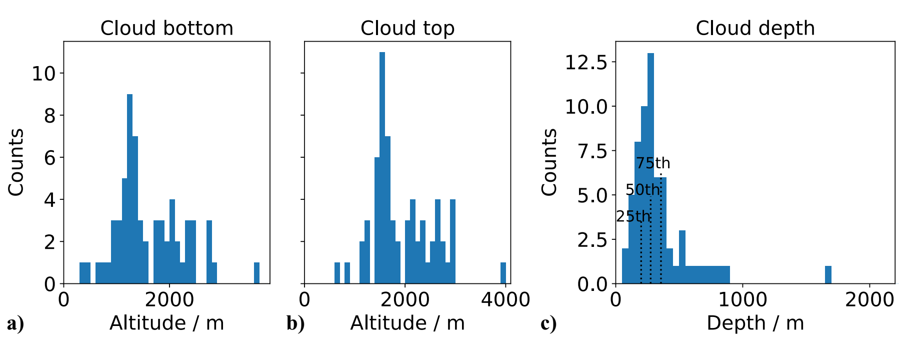

Fig. 2 Cloud bottom (a) and cloud top (b) altitudes and the associated cloud depth (c) during the North American campaign.

aircraft normally did not reach cloud bottom, such that the cloud bottom altitude stated here is the lowest altitude achieved by the aircraft within the cloud (the true cloud bottom altitude is unknown). The stated cloud bottom altitude may, therefore, in many of the cases, be an overestimate. Some ground observations are provided in [30], which indicate that icing conditions often extended down to a few hundred meters above ground level. These ground observations are not perfectly co-located in time and space with the aircraft measurements. Therefore, the incomplete profiles are shown to increase the number of cloud depth measurements. The available data shows that 25% of the clouds encountered in the North American campaign were thinner than 200 m (with the caveat that these profiles result from incomplete passages through the cloud). Another 25% of clouds had depths between 200 and 275 m, a further 25% had depths between 275 and 350 m, while the deepest 25% of clouds achieved up to 900 m, with one isolated case of 1700 m depth (see Fig. 2c). The average time from entry to exit of the icing conditions was 167 s.

B. European Flight Campaign

The European flight campaign took place in April 2023 and was based out of Toulouse, France (LFBF). The aircraft used for the measurements was the ATR 42 environmental research aircraft of the French facility for airborne research (SAFIRE) [31]. A total of 15 observational flights (OFs) were performed. The second test flight (TF) of the campaign, where all scientific airborne instruments were already operational, is also used to extend the dataset. The data of two observational flights (OF3 and OF4) are excluded from the evaluation due to a malfunction on the aircraft and at one of the instruments, respectively. The flights spent a total of 10 h and 40 min in icing conditions, of which 2 h and 29 min were in Appendix O conditions. An overview of the flights can be seen in Fig. 3 and in Table 2. The campaign's location in Toulouse allowed us to sample icing conditions formed in continental and maritime air masses.

The flights of the European campaign were either performed as Circulation Essais et Réception (CER) flights or as Airways flights.

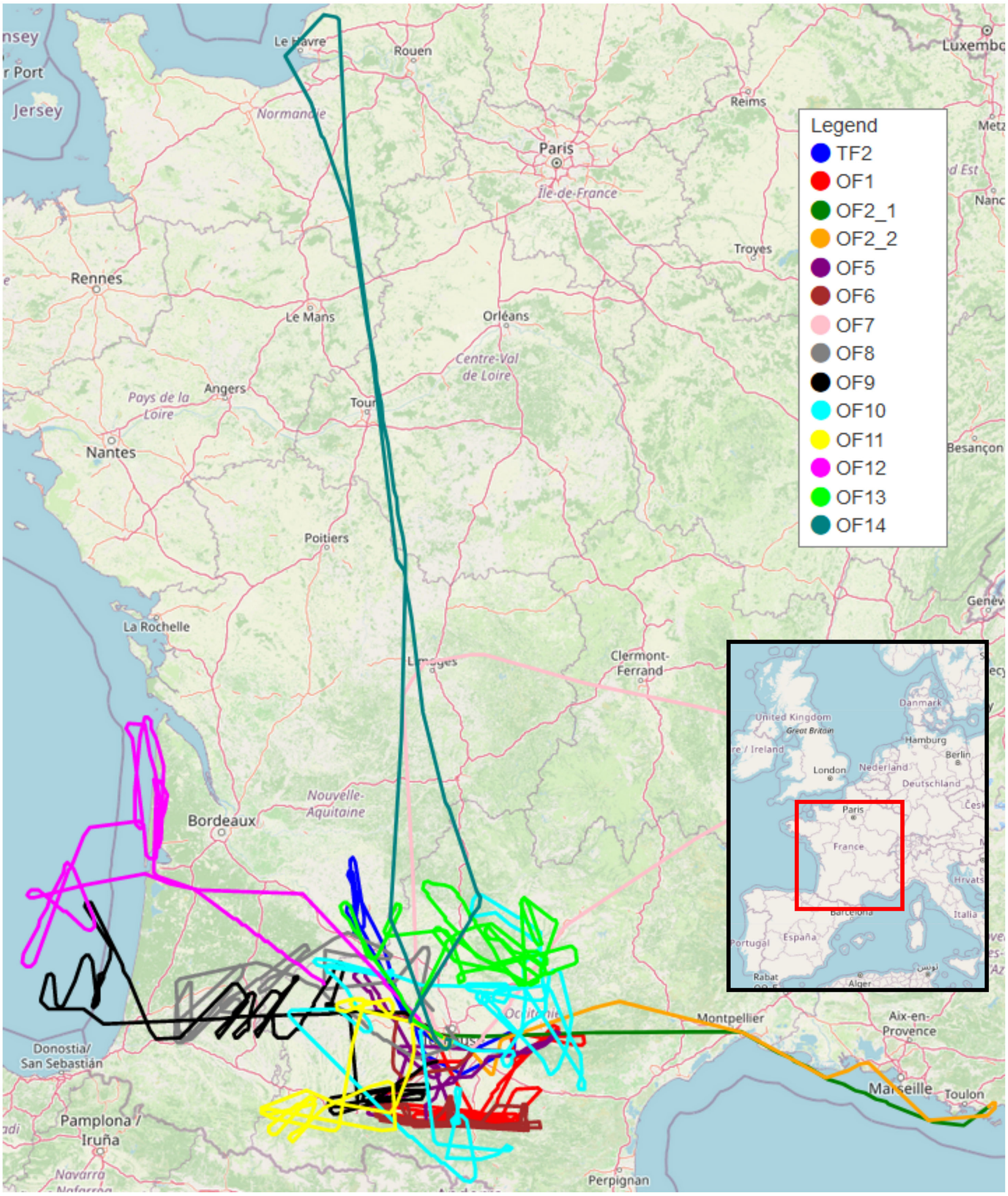

Fig. 3 Flights conducted within the European SENS4ICE campaign. Map from OpenStreetMap. The base of the flight operations was Toulouse.

Table 2 Flights of the European SENS4ICE campaign

Flight	Date	Flight time (UTC)	Flight type	Time in icing conditions [mm:ss]	Time in Appendix O conditions [mm:ss]	Airmass origin
TF2	24/03/23	09:30–11:05	CER	20:16	00:00	Maritime
OF1	03/04/23	06:08–09:38	CER	97:54	01:13	Continental
OF2_1	04/04/23	11:39–12:53	Airways	10:45	00:00	Continental
OF2_2	04/04/23	13:12–14:30	Airways	07:28	01:00	Continental
OF5	15/04/23	06:04–08:20	CER	46:37	18:32	Maritime
OF6	18/04/23	13:56–17:05	CER	77:36	00:00	Continental
OF7	20/04/23	10:40–13:20	Airways	16:20	00:00	Continental
OF8	22/04/23	06:03–08:52	CER	44:37	00:00	Continental
OF9	24/04/23	12:23–16:52	CER	88:49	55:00	Maritime
OF10	25/04/23	11:04–15:54	CER	91:42	39:41	Maritime
OF11	26/04/23	06:31–08:54	CER	17:31	00:00	Maritime
OF12	26/04/23	13:34–17:08	CER	54:56	08:43	Maritime
OF13	27/04/23	06:33–09:58	CER	60:52	09:01	Maritime
OF14	27/04/23	12:07–15:46	Airways	44:55	16:15	Maritime

The flight tracks are shown color-coded in Fig. 3. The implications of the airmass origin are discussed in Sec. V.B.

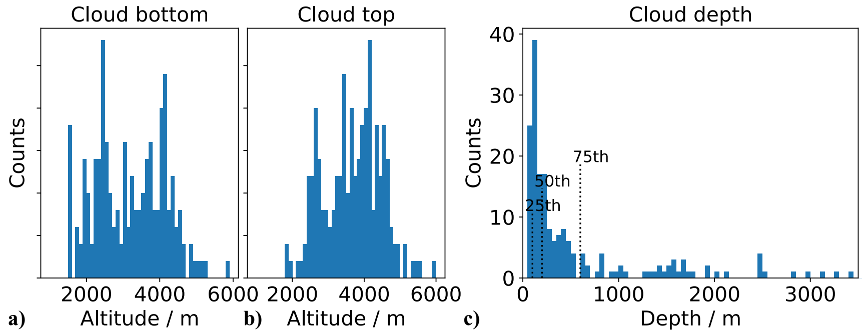

Fig. 4 Cloud bottom (a) and cloud top (b) altitudes and the associated cloud depth (c) during the European campaign.

CER refers to specifically designated areas that were reserved for the SAFIRE ATR 42. Flights in these areas were controlled by a dedicated air traffic controller; hence, there was flexibility for adjusting the flight plan. However, CER zones only existed in the vicinity of Toulouse and toward the Atlantic coast near Bordeaux. If no suitable weather conditions were predicted for these regions, airways flights were performed. In contrast to CER flights, airways flights had hardly any flexibility to make changes in the flight path or in altitude. During CER flights, the sampling of the clouds was mostly performed near cloud top, while for deicing, the SAFIRE ATR 42 descended to positive temperatures below the cloud. Cloud depths, computed similarly to those of the North American campaign, are shown in Fig. 4. The 25, 50, and 75 percentiles of cloud depth lie at 100, 200, and 600 m, with the top 25% of clouds attaining depths between 600 and 3450 m (Fig. 4c). The clouds in the European campaign were often patchy. Icing conditions lasted on average only 43 s, much shorter than the 167 s in the North American campaign. The patchiness makes it difficult to state where the sampling occurred with respect to cloud top. During airways flights, no deicing cycles were performed. The average speed of the ATR 42 during sampling was 110 $\mathrm{m\,s^{-1}}$.

III. Instrumentation

Key parameters for the description of icing and SLD conditions are the LWC and the droplet size distribution (DSD) [4]. The scientific instrumentation aboard the two research aircraft reflects the need to measure these two quantities. Hotwire probes were used to measure the LWC, as well as related properties, such as the TWC and the ice water content (IWC). DSDs were measured with a combination of scattering probes and optical array probes (OAPs). The following subsections describe the scientific instrumentation used during the two campaigns.

A. Instrumentation for the North American Flight Campaign

The Phenom 300 aircraft was equipped with an Ice Crystal Detector (ICD) for the measurement of LWC and TWC and a Cloud Combination Probe (CCP) for the particle size measurements. The ICD is a hotwire probe designed by Science Engineering Associates, Inc. (SEA) that has a convex sensor for the measurement of liquid droplets only and a concave sensor for the collection of ice and liquid water [32,33]. The CCP consists of two separate instruments, a scattering probe known as the Cloud Droplet Probe (CDP) [34–36] for the measurements of particles with diameters between 2 and 50 μm, and a Cloud Imaging Probe (CIP) for particles between 15 and 960 μm. The CDP derives the particle size from the intensity of forward scattered light that is measured at a photodiode. The CIP is an OAP [37,38], with a resolution of 15 μm. Particles that pass through a sample volume defined by the incident laser beam shadow a photodiode array. From the shadow images, the size and shape of the particles can be retrieved. The minimum size that can be measured with the CIP corresponds to one pixel of the diode array. The CIPs used in both flight campaigns were grayscale probes, i.e., they differentiate between multiple degrees of shadowing (25, 50, and 75%). Table 3 shows an overview of the instrumentation.

B. Instrumentation for the European Flight Campaign

The ATR 42 of SAFIRE was equipped with a large suite of scientific instruments from SAFIRE and the German Aerospace Center (DLR) (see Table 3) [39–42]. Measurements from three hotwire probes are available: from the LWC300 sensor [43,44], the Robust probe [45,46], and the Nevzorov probe [47]. The cylindrical LWC300 sensor measures only LWC; ice crystals are assumed to reenter the airflow after impact with the sensor. The Robust probe, on the other hand, has a single concave sensor (similar to that of the ICD) and measures only TWC [48]. Finally, the Nevzorov probe has three collector sensors, a concave sensor for LWC measurements, and two inverted conical sensors for the measurement of TWC [49]. Due to an

Table 3 Scientific instrumentation used in the SENS4ICE flight campaigns

Instrument	Measurement principle	Parameters measured	Owner
North American flight campaign			
CDP	Light scattering	Particle size (2–50 μm diameter)	Embraer
CIP	Imaging	Particle size and shape (15–960 μm diameter, grayscale)	Embraer
ICD	Hotwire	LWC, TWC (0.025[a]–10 $\mathrm{g\,m^{-3}}$)	SEA [33]
European flight campaign			
CDP	Light scattering	Particle size (2–50 μm diameter)	DLR [41,42]
CDP	Light scattering	Particle size (2–50 μm diameter)	SAFIRE [40]
CIP	Imaging	Particle size and shape (15–960 μm diameter, grayscale)	DLR [36,41]
CIP	Imaging	Particle size and shape (25–1600 μm diameter, monoscale)	SAFIRE [50]
PIP	Imaging	Particle size and shape (100–6400 μm diameter, monoscale)	DLR [42]
HSI	Imaging	Particle size and shape (20–2000 μm diameter)	DLR [51]
Nevzorov	Hotwire	LWC, TWC (0.025[a]–3 $\mathrm{g\,m^{-3}}$)	DLR [33,49]
LWC300	Hotwire	LWC (0.025[a]–3 $\mathrm{g\,m^{-3}}$)	SAFIRE [40]
Robust probe	Hotwire	TWC (0.025[a]–10 $\mathrm{g\,m^{-3}}$)	SAFIRE [50]

[a]The stated value is the lower threshold used for the evaluation of the SENS4ICE campaigns; it may be different for other evaluations.

instrument malfunction, Nevzorov probe data are available only for flights TF2, OF9, OF10, OF12, OF13, and OF14 (the evaluation of the hotwire sensors is described in Section IV.A).

For particle sizing, the ATR 42 carried two CDPs and two CIPs, one each from SAFIRE and DLR [36,41,50]. The data presented in this paper originates from the CDP and CIP of DLR. Comparisons between the CDPs of DLR and SAFIRE were performed and showed that the probes produce very similar results (see Appendix A). Due to their different resolutions (15 μm for the CIP of DLR and 25 for the CIP of SAFIRE), the CIPs are not comparable, and the CIP of DLR was selected for the evaluation due to its grayscale capabilities and higher resolution. Furthermore, a Precipitation Imaging Probe (PIP) was available. The PIP is an optical array probe like the CIP, but with a larger pixel size (100 μm) (hence lower size resolution) and a larger overall array width, allowing for the measurement of particles with sizes up to 6.4 mm. A high-resolution, High-Speed Imaging Probe (HSI) [51] was also flown, but its measurements were not used for this study due to the small sampling volume of the probe.

IV. Data Evaluation

This section first describes the data evaluation applied to obtain LWCs, DSDs, and particle size distributions (PSDs) for liquid and ice particles. Then, we explain how icing and Appendix O conditions were detected and characterized.

A. Hotwire Probes

Hotwire probes provide measurements of LWC and TWC by measuring the power needed to maintain a constant temperature [43]. This temperature was 175°C for the LWC300, 140°C for the ICD and the Robust probe, and 110°C for the Nevzorov probe. The power drawn by the instrument depends on the energy needed to heat and evaporate ice and water particles, but also on the convective heat losses. To derive LWC and TWC for hotwire probes, the convective heat losses need to be subtracted [47]. The convective heat losses can be estimated from flight segments in dry air, which can be identified by an analysis of the variations in the power signal. For this work, the analysis of the ICD data was performed by SEA. The analysis of the hotwire probes used in the European campaign was performed by the DLR. For each hotwire instrument evaluated by DLR, a database of all its measurements in dry air was established. The measurements were binned by airspeed, temperature, and pressure [52]. An average value of the convective heat loss was computed for each bin. For in-cloud segments, the convective heat losses were estimated by interpolating the binned (average) values for the exact pressure, temperature, and airspeed that were encountered. The procedure for the convective heat loss calculation differed slightly between the instruments, e.g., due to the different sampling rates at which they operated. In all cases, small offsets can remain in the residual power term after the removal of the convective heat losses, which can lead to slightly positive LWCs and TWCs in cloud-free segments (see Lucke et al. [49] for an estimate of the errors in the Nevzorov measurements). For this work, we assume that, given the uncertainty in the convective heat losses, we can identify the presence of clouds with an LWC or TWC above $0.025\ \mathrm{g\,m^{-3}}$. Segments with LWCs and TWCs below this limit are considered to be cloud-free.

The measurement accuracy of hotwire sensors also depends on their collision and capture efficiency [32,47,49,53,54]. The collision efficiency describes the ratio between the amount of water that impacts on the sensor and the amount of water that was contained in the volume upstream of the sensor. Especially small particles tend to follow the streamlines around the sensor, which leads to a collision efficiency smaller than 1. The capture efficiency describes how much of the water that impacts on the sensor is retained and evaporated. This depends on the sensor shape and the size and phase of the impacting particle. LWC sensors by design have a capture efficiency close to zero for ice particles [55]. On the other hand, droplet breakup on impact has also been observed to lead to lower capture efficiencies of liquid particles for LWC sensors, especially for larger drizzle drops [53]. TWC sensors have high capture efficiencies for SLDs and ice crystals. Lucke et al. [49] verified that capture efficiencies for SLDs with the Nevzorov probe are close to 100%. A study by Esposito et al. [33] found no indications of reduced capture efficiencies of SLDs for the ICD and the Robust probe either. However, for these two sensors, there are some indications that incomplete capture of ice crystals occurs [32] (see also Appendix B).

The LWCs and TWCs from the hotwire probes are denoted as $\mathrm{LWC_{HW}}$ and $\mathrm{TWC_{HW}}$, respectively. For the North American campaign, these values always originate from the ICD concave and convex sensors, respectively. For the European campaign, the $\mathrm{LWC_{HW}}$ stems from the LWC300 sensor. The $\mathrm{TWC_{HW}}$ originates from the 8 mm TWC cone of the Nevzorov probe and from the Robust probe for the flights where the Nevzorov probe did not work. An analysis of PSDs and TWCs indicated that the Nevzorov probe is more efficient at capturing ice crystals than the Robust probe; therefore, the Nevzorov 8 mm cone TWC data are used where available.

B. Evaluation of Particle Size Measurements

To obtain PSDs and DSDs from the particle sizing instrumentation, two tasks need to be performed:

1) Separation of liquid and nonliquid particles from the images

2) Combination of the size distributions from the individual instruments

The separation of liquid and nonliquid particles is performed for each probe individually. The CDP measures just a single intensity value. No information on the particle shape can be derived from this measurement. For the data evaluation, it is assumed that all measured particles are liquid and spherical. For clouds with a significant LWC, this is a reasonable assumption, given that cloud condensation nuclei (CCNs) are much more abundant than ice nucleating particles. Hence, the ratio of small droplets to small ice crystals tends to be high in mixed-phase clouds [56–59].

C. Particle Classification with the CIP

The CIP is the key instrument to discriminate between Appendix O and SLD-free (Appendix C) icing conditions. This was done by an analysis of the particle images. The diameter D of a particle is defined as the diameter of the minimum enclosing circle [60], unless mentioned otherwise. For out-of-focus particles, a correction according to Korolev [61] was applied. Only particles that were completely imaged were considered for the analysis. Additionally, the data were corrected for stuck bits and shattering artifacts [62]. A procedure to separate coincident droplets in image frames was also applied. The minimum size that can be measured with the CIP corresponds to one pixel (px) of the diode array. Naturally, no shape information can be retrieved from a single-pixel measurement. The shape differentiation is therefore only possible above a certain particle size. An in-house code of DLR [16,36,62] was used to design filters that distinguish four categories of particles:

1) Small particles: All particles with $D < 6$ px (i.e., smaller than 97.5 μm under consideration of the resolution of 15 μm). All small particles are considered to be liquid particles, which is justified similarly as for the CDP (see Sec. IV.B).

2) SLDs: For SLDs, special filters were designed that assess the roundness of the particle images. Parameters that are considered for the roundness are, e.g., the shaded area in the outermost 10% of the enclosing circle radius, the aspect ratio, and the ratio between the shaded area within the smallest enclosing circle and the overall circle area. A detailed description of the filters can be found in [63]. SLDs are by definition liquid.

3) Large aspherical particles (LAS): This category is used to detect the presence of ice particles. It is not intended to detect all ice particles but to detect ice particles with very high confidence. The respective filters select particles for which less than 60% of the area within the smallest enclosing circle is shaded and particles for which the shading patterns at grayscale levels 50% and 75% exhibit large differences between the x- and y-directions.

4) Other ice particles: Particles with $D \geq 6$ px that meet neither the requirements for SLDs nor those of LAS. These particles are also classified as ice particles, but the confidence in the classification is lower than for the LAS category.

The classification is associated with errors. Especially difficult to classify are particles that are imaged out of focus [64]. The number of out-of-focus images can be reduced by restricting the depth of field (DOF), which is defined as [38]

$$\mathrm{DOF}(\chi) = 2c(\chi)\frac{D}{4\lambda} \tag{1}$$

where λ is the laser wavelength. The value χ represents a requirement on the shadowing level that a particle image needs to have to be counted [38]. We differentiate three depth-of-field settings, as described by Menekay [63] and based on Lilie et al. [65]:

1) Mode 1: All particle images that have at least one pixel at the 50 or 75% shadow level are accepted. This corresponds to a value $c = 8.18$.

2) Mode 2: All particle images that have at least one pixel at the 75% shadow level are accepted. This corresponds to a value $c = 3.68$.

3) Mode 3: All particle images that have more than 50% of their pixels shadowed at the shadow level of 75% are accepted. This corresponds to a value $c = 0.9$.

By selecting more restrictive DOF criteria, the number of measured particles is reduced by a factor of approximately 2.1 when selecting mode 2 instead of mode 1 and by a factor of 4 when selecting mode 3 instead of mode 2. The choice of the suitable threshold is therefore a tradeoff between sample size and image quality.

One can think of the particle images that result from these DOF settings as datasets. The mode 1 dataset contains all particle images. The mode 2 dataset is a subset of the mode 1 dataset, while the mode 3 dataset is a subset of both the mode 1 and mode 2 datasets. To establish the classification accuracy for the mode 2 and mode 3 datasets, we manually selected two segments, one that contained almost exclusively SLDs and another one that contained almost exclusively ice crystals. Then, we ran the particle classification on both segments, once using the mode 2 dataset and once using the mode 3 dataset. The results are shown in Fig. 5. Only the classification of large particles ($D \geq 6$ px) is depicted, because the separation of small and large particles is straightforward. The left column shows the classification of images in the segment that contained predominantly SLDs. With the mode 2 dataset, 97% of the particles are classified as SLDs, 0.3% as LAS (large aspherical particles), and 2.7% as other ice particles. The detection of SLDs is therefore reliable. With the mode 3 dataset, the detection of SLDs works even better; only 1.0% are classified as other ice particles. Thus, by using the mode 3 dataset instead of the mode 2 dataset, the retrieval of the SLD number concentration can be slightly improved. For both datasets, the particles classified as LAS are assumed to be correctly identified and thus represent ice particles that were occasionally present during the segment.

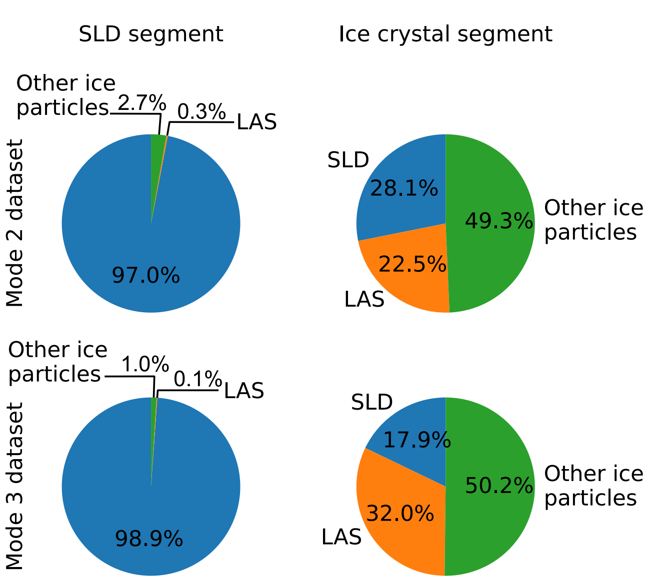

Fig. 5 Classification of CIP images of particles with $D \geq 6$ pixels in clouds dominated by SLDs (left) and ice crystals (right) for the mode 2 (top) and the mode 3 (bottom) datasets.

The right column shows the classification of particles for the segment that consisted mostly of ice particles. It is important to understand that even during a visual assessment of the images, not all particles can be unambiguously identified, and some SLDs can be present in the ice crystal segment. For the mode 2 dataset, 22.5% of particles were identified as LAS, 49.3% of particles were identified as other ice particles, and 28.1% were identified as SLDs. Hence, approximately 71.8% of particles were correctly identified. For the mode 3 dataset, 82% of particles were correctly identified, and the false detection of SLDs is significantly reduced compared to the mode 2 dataset. The detection of LAS increases from the mode 2 to the mode 3 dataset, likely because the filters for LAS are partly also designed to select well-focused particles.

For this study, the mode 3 dataset was used for the detection of SLDs. Despite the restrictive filtering associated with mode 3, the number of SLDs, even in samples with relatively low number concentrations, was sufficient to derive microphysical parameters, and, importantly, using the mode 3 dataset reduces the false detection of SLDs. Additionally, it provides a small advantage in the detection of SLDs; 99% of particles are detected as SLDs, compared to 97% in the mode 2 dataset. For LAS, the mode 2 dataset was used. Aspherical particles come in very different shapes; hence, a strict requirement on the ratio between the number of pixels at the 75% level and the 50% level is not useful. Since LAS only serves as an indication of the presence of ice particles, the numerical values are less important. The other ice particles were also identified from the mode 2 dataset in order to be able to measure relatively low concentrations of ice particles. Due to the misclassifications of SLDs, the number concentration of ice particles is more uncertain than that of SLDs. According to Fig. 5, the number concentration of all ice particles (LAS and other ice particles) can be underestimated by up to 28.1%.

The small particles were computed from the mode 2 dataset for the American campaign and from the mode 1 dataset for the European campaign. For the European campaign, it was found that the number concentrations in the uppermost CDP bins exceeded those in the lowermost CIP bins significantly if the mode 2 dataset was used [63]. This difference was attributed to an error with the CIP, because both CDPs, that of SAFIRE and that of DLR, agreed on the larger number concentration. The offset between CDP and CIP was significantly smaller if the mode 1 dataset was used; hence, it was decided to select the small droplets from the mode 1 dataset for the European campaign. This yields realistic size distributions but does not clarify the reason for the offset. The offset was not observed for the American campaign; hence, there the number of small droplets was computed from the mode 2 dataset.

D. Particle Classification with the PIP

For the European flight campaign, data from the PIP were used to extend the available size distributions toward diameters up to 6400 μm. Unlike the CIP, the PIP is a monoscale probe, i.e., a pixel can only have two values, illuminated or shadowed (shadowed corresponds to an intensity decrease of more than 50%). Only particles with diameters equal to or larger than 600 μm (i.e., a minimum of 6 px), were considered, as the CIP covers the size range below that value (as is explained in the subsequent section). Similarly, as for the CIP (see Sec. IV.C), an algorithm was applied to distinguish ice particles from liquid particles. The contribution of the PIP to the size distributions of liquid particles was negligible; hardly any drops larger than 600 μm were encountered. The PIP data mostly serve to obtain the complete size range of ice particles.

E. Combination of Particle Size Distributions

For both flight campaigns, the data from the CDP [34,35] and CIP needed to be combined. In the case of the European flight campaign, measurements from the PIP were also included. The PSDs therefore extend from 2 to 960 μm for the North American campaign and from 2 to 6400 μm for the European campaign.

The threshold between the PSDs of CDP and CIP was set to 43 μm. This allowed us to discard the lowest two size bins of the CIP, which are associated with a large uncertainty due to the small DOF value of small particles and the large relative errors that exist due to the size resolution of 15 μm of the CIP. The first CIP bin used has a midpoint diameter of 45 μm, which corresponds to a length of three adjacent pixels.

The threshold between the PSDs of CIP and PIP was set to 600 μm. Due to the requirement to have particles fully imaged, the sampling statistics of the CIP would get very poor if a higher threshold was used. On the other hand, a lower threshold would have carried the risk of confusing SLDs and ice crystals due to the low resolution of the PIP.

The combined size distributions were used to derive characteristic parameters, such as the MVD as well as the VD_{90} and VD_{99} (the diameters for which 10 and 1% of the volume of liquid water in the cloud is contained in droplets larger than the stated diameter, respectively).

The accuracy of these characteristic parameters, which is of large importance for the description of the severity of icing conditions, depends on the separation of liquid and nonliquid particles that was explained previously. If many ice particles are misidentified as SLDs, the mass contained in SLDs and consequently also the MVD, VD_{90}, and VD_{99} are overestimated. Vice versa, if many SLDs are detected as ice crystals, the measured MVD, VD_{90} and VD_{99} values may be too low.

F. Detection and Classification of Icing and Appendix O Conditions

In-situ conditions are classified as icing conditions when the LWC from the hotwire instrument exceeded the sensitivity threshold of $0.025\ \mathrm{g\,m^{-3}}$ and the static air temperature (SAT) of the ambient air was less than 0°C. The icing classification (a.k.a. flag) does not consider the ram air temperature rise due to the pressure increase, which prevented ice accretion on aircraft surfaces when SAT was just slightly less than 0°C. However, as this work aims to describe icing conditions irrespective of the aircraft type, the 0°C threshold is considered appropriate.

The assessment of the presence of Appendix O conditions is more complex. For SENS4ICE, Appendix O conditions are considered to be present when the following conditions are met:

1) The static air temperature (SAT) must be smaller than 0°C.
2) The LWC measured by the hotwire instrument (LWC_{HW}) must be larger than $0.025\ \mathrm{g\,m^{-3}}$.
3) The diameter that marks the 99th percentile of the cumulative volume distribution (VD_{99}) must be larger than 100 μm.
4) The ratio of LWC to TWC of the hotwire instruments (LWC_{HW}/TWC_{HW}) must be larger than 0.4.
5) The number concentration of large aspherical particles (N_{LAS}) must be smaller than $1000\ \mathrm{m^{-3}}$.
6) The number concentration of SLDs must be 10 times larger than that of LAS ($N_{SLD} > 10N_{LAS}$).
7) The number concentration of SLDs must be larger than $100\ \mathrm{m^{-3}}$.

The first condition implements the same temperature threshold as for the standard icing conditions. The second condition represents the threshold sensitivity of the hotwire sensor. Usage of a lower threshold can result in an erroneous flag, e.g., when rapid changes in the convective heat losses occur. The third condition establishes a distinction of Appendix O conditions based on the percentage of the water volume contained in drops larger than 100 μm. Icing conditions are only considered to be SLD conditions if more than 1% of the overall liquid water content is contained in SLD. The fourth and the fifth conditions, which are loosely based on Cober and Isaac [4], aim to identify flight segments where a high number of ice crystals are present, of which a few are misidentified as SLDs, such that the segment is falsely classified as Appendix O. We acknowledge that, due to conditions four and five, the detection of Appendix O conditions may be missed when many large ice crystals and SLDs coexist. Not applying conditions four and five would risk severely overestimating parameters such as the MVD in Appendix O conditions that contain ice particles. Therefore, it was preferred to exclude Appendix O conditions with a high number of ice crystals. Similarly, the sixth condition ensures that SLD conditions are not triggered when the ratio of SLDs to ice crystals is relatively low (below or equal to 10), where it would be likely that misidentified ice crystals distort the microphysical parameters computed for the SLDs. The last condition is used to prevent false alarms in cases where just a few particles are detected overall. In such conditions, ice crystals can be mistaken for SLDs without triggering the fifth or the sixth condition. The threshold is justified because even if SLD conditions were missed due to the condition, the LWC contained in the SLDs (assuming a droplet diameter of 250 μm) would be only $0.0008\ \mathrm{g\,m^{-3}}$, and thus negligible.

The output of our evaluation provides data at a resolution of 1 s. To ensure a robust detection, all parameters used in the conditions, except for the SAT and the LWC threshold for the general icing conditions, are based on rolling averages of 15 s (computed for each second), with the value at time t being the average of the individual 1 s values from the time window $t-7$ to $t+7$ s. The data that are presented in the Results section (Sec. V) are based on the separation of icing and Appendix O conditions that was explained in this section.

G. Definition of Encounters

The previous section described the detection of SLD conditions. As atmospheric conditions can fluctuate rapidly, the presence of icing and SLD conditions can also change from one second to the next. This can happen even though 15 s averages are used, e.g., when the VD_{99} fluctuates around 100 μm. For the investigation of icing events and the study of the related microphysical parameters, it can be helpful to look at a longer encounter than at the individual values observed per second. Therefore, we grouped icing and SLD conditions into encounters. These were defined as follows:

1) An encounter needs to be at least 5 s long.
2) An encounter is terminated after the required condition (icing or Appendix O conditions) is not detected for more than 5 s. The end of the encounter is then set to the time when the respective condition was last detected.

V. Macro- and Microphysical Properties of Icing Conditions

This section presents the macro- and microphysical properties of the icing conditions that were observed during the North American flight campaign and the European flight campaign. When comparing the results, it is important to remember the different seasons and locations where the studies were performed (see Tables 1 and 2). At first, we describe general properties of the icing conditions like altitude, temperature, and LWC (Sec. V.A). Then, we investigate the microphysical properties of Appendix O conditions in more detail (Sec. V.B). Subsequently, we also analyze the microphysical properties of the mixed-phase conditions that we encountered and discuss their formation (Sec. V.C). In the end, we compare our observations to the Appendix O regulations [8] (Sec. V.D).

A. Altitude and Temperature of Icing Conditions

In Fig. 6, the altitude of icing conditions (grouped into bins of 500 m), the LWC measured by the hotwire sensor, and the time spent in Appendix C and O conditions are plotted. During the North American campaign, most icing conditions were encountered between 1000 and 3000 m; this is also where the highest LWCs were encountered (see Figs. 6a and 6b). LWCs were on average between 0.25 and $0.5\ \mathrm{g\,m^{-3}}$ in that altitude range for both Appendix C and Appendix O conditions. In Appendix C conditions, LWCs

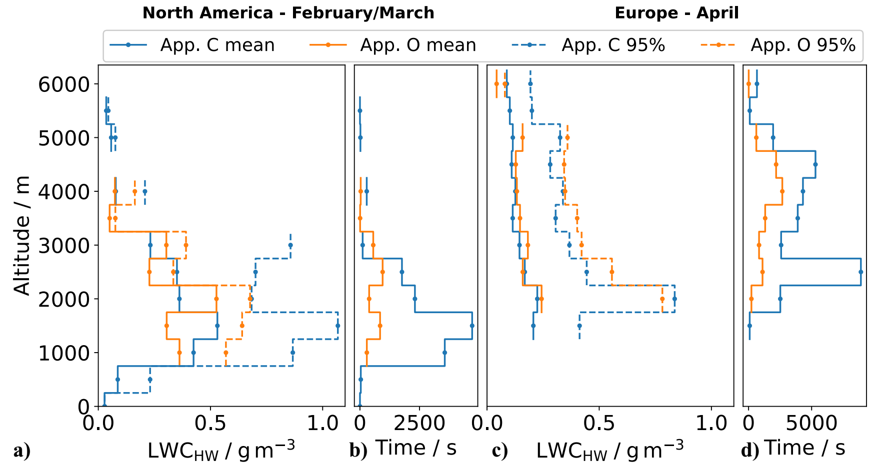

Fig. 6 Altitude and LWC of Appendix C and O conditions for North America and Europe. Panels a) and c) show means and 95th percentiles of LWC_{HW}. Panels b) and d) display the time spent in icing conditions per altitude bin.

occasionally reached more than 1 $g\,m^{-3}$, while LWCs in Appendix O conditions sporadically attained up to 0.6 $g\,m^{-3}$.

As would be expected due to the warmer surface temperatures, icing altitudes during the European campaign in spring were higher than during the North American campaign in the winter months. Figures 6c and 6d show that in the European campaign, no significant icing was encountered below 1500 m. During this campaign, icing conditions between 1500 and 3000 m were sampled, especially during the first flights (TF2, OF1–OF6), while later flights (OF7–OF14) sampled predominantly midlevel clouds at altitudes between 3000 and 6000 m. The average LWCs during the European campaign were between 0.15 and 0.25 $g\,m^{-3}$ and decreased slightly with altitude. LWCs in Appendix O conditions tended to be slightly higher. The 95th percentile LWCs show maxima at 2000 m for both Appendix C and Appendix O conditions that are due to severe icing experienced in OF1. For altitudes between 3000 and 5000 m, the 95th percentile LWCs decrease slowly from 0.37 to 0.32 $g\,m^{-3}$ for Appendix C conditions and from 0.42 to 0.36 $g\,m^{-3}$ for Appendix O conditions.

The data shown in Fig. 6 are affected by the sampling strategy of the two campaigns. In the North American campaign, where the aircraft entered mostly thick stratus clouds from cloud top and, after sampling, escaped via the cloud top, icing conditions deeper in the cloud may not be properly represented. Similarly, icing conditions found toward cloud base are likely underrepresented in the European campaign, where the sampling took place mostly at cloud top, but the aircraft exited through the cloud base for deicing.

The probability of clouds containing icing conditions, rather than glaciated conditions, decreases with decreasing temperature [66]. Figure 7 depicts the temperature (in bins of 2°C) versus the LWC and the time spent in icing conditions during SENS4ICE. Figure 7b shows that the large majority of samples during the North American campaign were collected at temperatures between −4 and −13°C, with a maximum between −7 and −9°C (34%). For the European campaign (Fig. 7d), the measurement range was centered around slightly warmer temperatures, with a maximum number of measurements taken between −3 and −5°C (31%). Three percent of the conditions were sampled at temperatures between −11 and −13°C. The absence of a large number of measurements between −3 and 0°C is intentional, as one of the goals of the SENS4ICE campaigns was also to assess the aircraft performance with ice accretion; SATs that corresponded to positive total temperatures near the aircraft fuselage were avoided. Only 1.6 and 2.1% of all icing conditions had temperatures below −13°C in the North American and the European campaign, respectively. This reflects the meteorology during the two campaigns but does not mean that icing conditions below −13°C are generally unlikely.

Regarding the relationship between LWC and temperature, no clear trend is perceptible for the North American campaign (Fig. 7a). Average LWC values for temperatures between −12 and 0°C vary between 0.28 and 0.53 $g\,m^{-3}$ for Appendix C conditions and between 0.29 and 0.41 $g\,m^{-3}$ for Appendix O conditions. The 95th percentile values vary between 0.61 and 1.06 $g\,m^{-3}$ for Appendix C and between 0.39 and 0.70 $g\,m^{-3}$ for Appendix O. The LWC for Appendix O conditions appears to be higher for warmer temperatures; this matches the description in Cober and Isaac [4]. For the European flight campaign (Fig. 7c), average LWC values in Appendix C conditions decrease slightly from 0.16 $g\,m^{-3}$ at −2°C

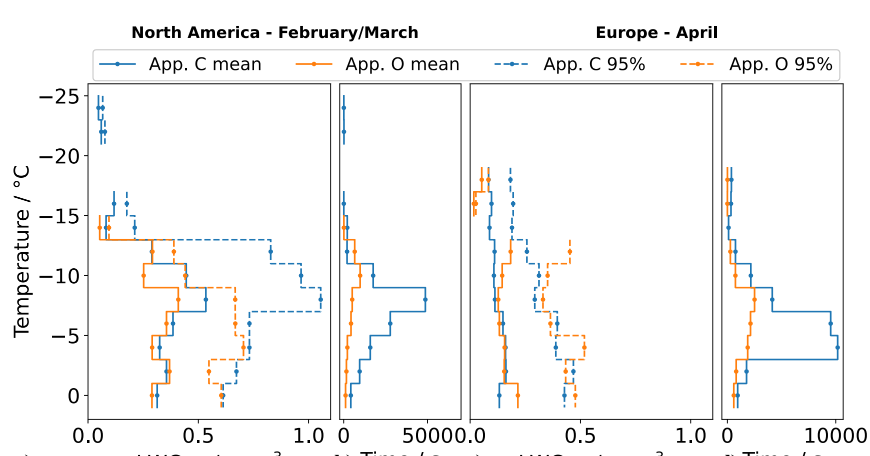

Fig. 7 Temperature and LWC of Appendix C and O conditions for North America and Europe. Plots a) and c) show the means and 95th percentiles of LWC_{HW}. Plots b) and d) display the time spent in icing conditions per temperature bin.

to 0.11 $g\,m^{-3}$ at $-12°C$. On the other hand, the average LWCs in Appendix O conditions do not decrease with decreasing temperature but even attain a value of 0.18 $g\,m^{-3}$ at $-12°C$. The 95th percentiles of LWC in Appendix O conditions even exceed those of Appendix C for most points in the temperature range. While a relatively clear decrease from 0.47 $g\,m^{-3}$ at $-2°C$ to 0.26 $g\,m^{-3}$ at $-12°C$ can be observed for the Appendix C 95th percentile, no such trend is perceptible for Appendix O conditions, and the 95th percentile attains a relatively high LWC value of 0.45 $g\,m^{-3}$ at $-12°C$.

B. Number Concentrations and Droplet Size Distributions of Appendix O Conditions

Apart from the LWC and temperature, particle size distributions and derived parameters like the MVD, VD_{90}, and VD_{99} and also the LWC that is contained in the SLDs are important quantities to judge the severity of icing conditions. Typical size distributions for SLD conditions were published in Cober and Isaac [4]. Figure 8a shows the cumulative mass distributions of the Appendix O encounters of the North American campaign. Also plotted are the distributions for the FZDZ Appendix O icing environments with MVD < 40 and MVD > 40 μm [4]. For all but one of the cumulative mass distributions, more than 80% of the LWC is contained in droplets with diameters smaller than 100 μm. The MVD of the mean curve is 23 μm. Predominantly FZDZ conditions with MVD < 40 μm were sampled, and the mean curve matches that for FZDZ MVD < 40 μm in the Appendix O regulations [4,8] closely. This is likely related to the sampling strategy (see Sec. II.A) that was designed to maximize safety. The procedure of entering and exiting the cloud through the top means that most of the Appendix O sampling occurred near the cloud top, where the small drop contribution to Appendix O clouds tends to be dominant, frequently resulting in MVD < 40 μm. Appendix O clouds with MVD > 40 μm tend to occur well below the cloud top, often near or below the cloud base, where the small drop contribution to the drop size spectrum is much smaller, and drizzle has grown to larger sizes through collision coalescence.

The cumulative distributions of the Appendix O encounters of the European campaign can be seen in Fig. 8b. Many more encounters occurred than in the North American campaign. This is partly due to the larger number of flight hours in the campaign but also because the clouds in the European campaign were patchier than during the North American campaign (Appendix O encounters in Europe were often shorter than one minute). The European campaign data contains many cumulative mass distribution curves with MVDs around 45 μm. The mean curve and most of the individual curves match neither the typical curve of the FZDZ MVD < 40 μm nor that of the FZDZ MVD > 40 μm regime. Especially, the amount of liquid water contained in droplets with diameters smaller than 20 μm is much lower than for most cases of the North American campaign and the Cober and Isaac [4] studies. Furthermore, the curves observed in the European campaign often do not exhibit bimodality but appear to have just one maximum in the first derivative.

Another fundamental property for the description of clouds is the number concentration N. In Fig. 9, N is plotted against the altitude for each Appendix O condition in the two campaigns, with marker size and color corresponding to the concentration and the MVD of SLDs during the event, respectively. The plot contains some of the information already portrayed in Fig. 6 but adds information on the droplet and SLD number concentrations and the size of the SLDs. For the North American campaign (panel a), all encounters fall on the right side of the plot, with number concentrations ranging between 20 and 300 cm^{-3}. For the European campaign (panel b), the opposite is the case; the large majority of encounters have number concentrations below 20 cm^{-3} and at times as low as 0.5 cm^{-3}. A comparison of the sizes of the markers shows that the number concentrations of SLDs fluctuated widely (which is to be expected), but the mean number concentration of the two campaigns was relatively similar, with

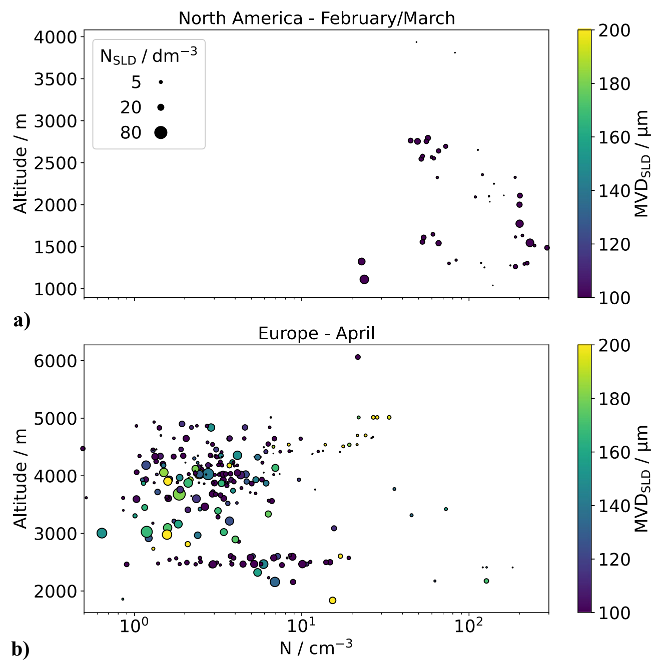

Fig. 9 Number concentration (N) and altitude of Appendix O conditions in the North America (a) and Europe (b). The marker area and marker color specify the concentration and MVD of the SLDs, respectively.

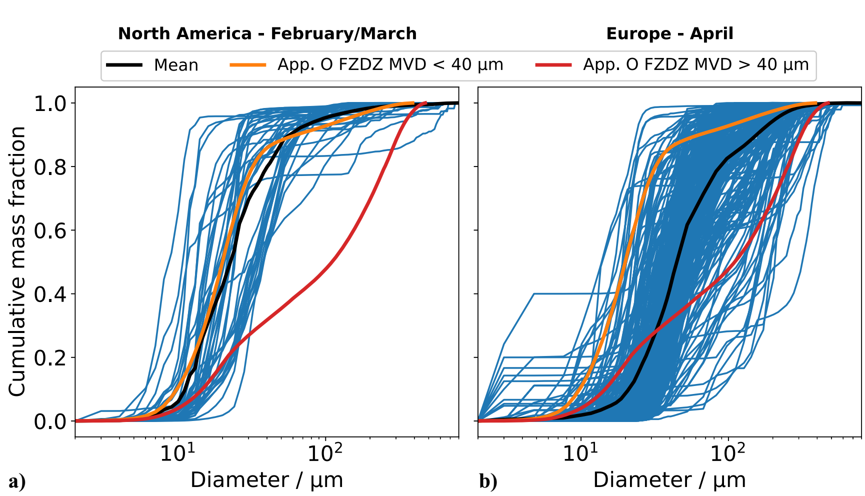

Fig. 8 Cumulative mass distributions for the Appendix O encounters of the North American (a) and European flight campaign (b), with mean curves plotted in black. Mean cumulative mass distributions for freezing drizzle MVD < 40 and MVD > 40 μm from Cober and Isaac [4] are plotted in orange and red, respectively.

8 dm^{-3} in North America and 12 dm^{-3} in Europe, respectively. The maximum number concentrations were 40 and 79 dm^{-3} for North America and Europe, respectively. The color code shows that SLDs attained larger sizes during the European campaign. While the MVD of SLDs in the North American campaign only exceeds 120 μm in very few cases, during the European campaign a wide range of values from 100 μm to more than 200 μm are observed.

C. Presence of Mixed-Phase Clouds

For the forecast and nowcast of icing conditions, it is important to understand when a cloud transitions to a mixed-phase regime and the spatial extent over which this occurs. There is no universally accepted definition of a mixed-phase cloud [66]. For this study, we detect a mixed-phase cloud when $N_{LAS} \geq 1000\ m^{-3}$. N_{LAS} is the number concentration of large aspherical particles, which can be seen as an indication for the number concentration of ice particles that grew to sizes beyond 97.5 μm (6 pixels of the CIP). According to the detection procedure (see Sec. IV.F), the mixed-phase conditions presented here cannot be Appendix O conditions, i.e., they are all identified as Appendix C conditions. Figure 10 shows the altitude and total number concentrations (ice and water) of all mixed-phase clouds encountered in the SENS4ICE campaigns. The marker size corresponds to the number of ice crystals, and the color provides the MVD of droplets smaller than 50 μm (only small drops are considered such that ice crystals misidentified as SLDs do not influence the MVD). The majority of mixed-phase observations originate from the European campaign. Most of the observations from the North American campaign (panel a) were purely liquid, and the few mixed-phase observations tended to fall toward the lower-right corner; they occurred at low altitudes in clouds with high number concentrations (on average 271 cm^{-3}), i.e., they were dominated by supercooled droplets. The mixed-phase encounters from the European campaign (panel b) appear to be layered, this is a manifestation of the altitude of flights during which many mixed-phase conditions were sampled. The overall number concentrations (number of ice and liquid particles) of these mixed-phase clouds are low (on average 18 cm^{-3}), similar to the number concentrations observed for many of the Appendix O conditions from the European campaign (see Fig. 9). However, the number concentration of ice alone in many mixed-phase encounters accounts for several percent of total N in the European campaign, comparable to that of the SLDs during the Appendix O encounters. MVDs of the simultaneously existing supercooled droplets are relatively large, often between 30 and 40 μm. Possible causes for the formation of ice crystals are discussed in Sec. VI.C.

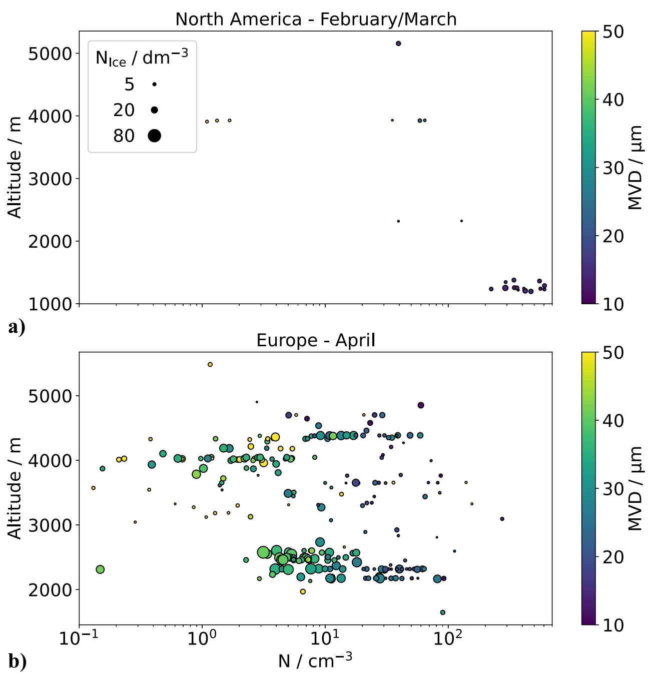

Fig. 10 Number concentration of all particles (N) and altitude of mixed-phase conditions for North America (a) and Europe (b). The marker area is proportional to the concentration of ice particles, while the marker color specifies the MVD of the small supercooled droplets.

D. Comparison to the Appendix O Certification Envelopes

For aircraft certification, it is important how the collected data compare to the certification envelopes of Appendix O. The certification envelopes describe the conditions in which aircraft must be shown to safely operate. All environmental conditions found to lie outside these envelopes are a concern because then an aircraft could encounter an environment for which its safety of flight is not proven. Two different envelopes for FZDZ are specified in Appendix O: A pressure altitude-temperature envelope and an LWC-temperature envelope. The LWC-temperature envelope is subdivided into an envelope for FZDZ MVD < 40 and FZDZ MVD > 40 μm [8]. Figure 11 shows the pressure altitude and temperature data from the Appendix O encounters of the North American and European flight campaigns plotted into the corresponding envelope of Appendix O. No points fall outside the envelope. The ensemble of data points from the European campaign follows the slope of the envelope. Thus, the envelope agrees well with the conditions encountered during SENS4ICE.

For the comparison of the LWC of the Appendix O encounters to the certification envelopes, the duration (and the corresponding distance traveled) needs to be considered. The certification envelopes represent averages over 17.4 nautical miles; if data with different encounter lengths are evaluated, a scaling factor needs to be applied to the LWC [4]. For instance, the average LWC measured during an encounter with a horizontal extent of 3000 m needs to be

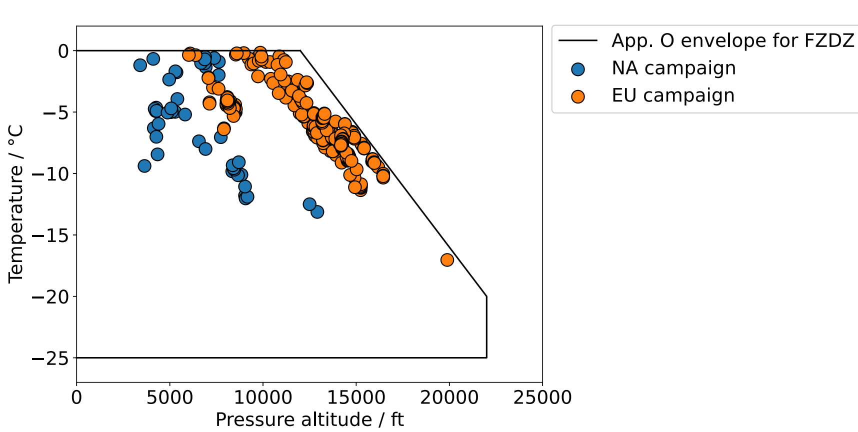

Fig. 11 Pressure altitude and temperature of the Appendix O encounters from North America and Europe plotted into the pressure altitude-temperature envelope from the Appendix O regulations.

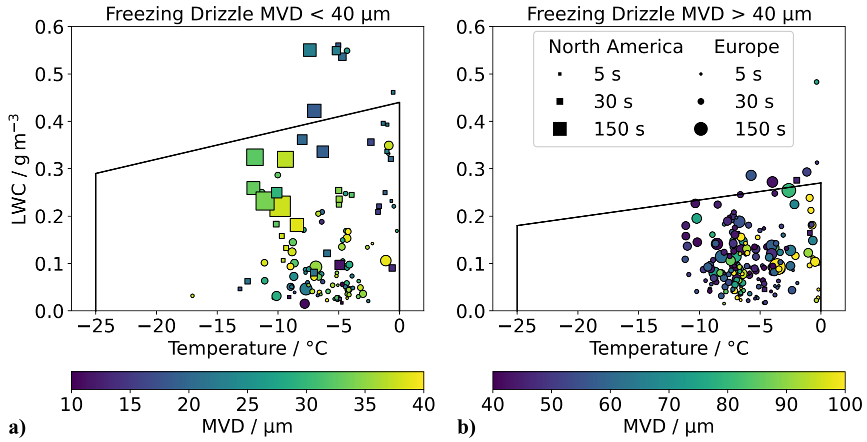

Fig. 12 LWCs of Appendix O conditions for encounters with MVD < 40 μm (a) and MVD > 40 μm (b). The size and color of the markers reflect the duration and MVD, respectively.

multiplied by 0.82 before it is compared to the LWC envelopes of Appendix O (see CS-25, Appendix O [9] for the calculation of the scale factor). This scaling reflects the decreasing probability of encountering high LWC over long distances. The comparison of the LWC of the Appendix O encounters from the two flight campaigns with the certification envelopes can be seen in Fig. 12. The appropriate scaling factors were applied to all encounters. The markers were sized according to the duration of the encounter and colored according to the MVD.

The large majority of the Appendix O encounters with MVD < 40 μm fall within the respective FZDZ envelope. A total of seven of the 127 encounters lie outside of the envelopes. Of those, one occurred at a temperature close to 0°C, likely causing no ice accretion at the aircraft, while another is still fairly close (within 6%) of the envelope. Five more are found at temperatures between −4 and −7°C, with LWCs between 0.54 and 0.56 g m^{-3} (distance-adjusted values) and MVDs between 18 and 26 μm. The encounters that originated from the North American campaign were usually several minutes long, while encounters from the European campaign often lasted less than 1 min. Of the 176 Appendix O encounters with MVDs > 40 μm, a total of six fall outside the FZDZ MVD > 40 μm envelope, five of which are still relatively close (within 10%) to the envelope or at a temperature between −1 and 0°C. The encounter that exceeded the envelope significantly had an LWC of 0.29 g m^{-3} (distance-adjusted value), an MVD of 56 μm, and occurred at a temperature of −6°C. Most of the FZDZ conditions with MVD > 40 μm originate from the European flight campaign, likely due to the maritime origin of the air masses in which many of the clouds were sampled (see Sec. V.B). Again, like for the conditions with MVD < 40 μm from the European campaign, the encounters were relatively short, only sporadically exceeding one minute.

VI. Discussion and Outlook

This work has presented detailed information on the icing conditions observed during two flight campaigns in North America and Europe in the winter and spring of 2023. Here, we discuss the findings and their implications.

A. Temperature and Altitude of Icing Conditions

The temperatures and altitudes of icing and Appendix O conditions observed in the two campaigns largely match previous observations. Temperatures below −12°C were rarely encountered; as stated previously, this reflects the meteorological conditions during the two campaigns. The absence of measurements below −12°C does not mean that Appendix O conditions below this temperature are in general rare. The observations also matched the pressure altitude-temperature envelope of Appendix O well, thus substantiating the previous findings.

B. Reasons for Differences Between Appendix O Conditions in North America and Europe

This section discusses possible reasons for the smaller number concentrations and larger MVDs observed for the Appendix O conditions in the European campaign compared to the North American campaign, as presented in Sec. V.B.

Two processes are involved in the formation of FZDZ conditions:

1) Diffusional growth of droplets
2) Collision-coalescence processes

Cloud droplets initially grow in water-supersaturated air through diffusion. SLDs generally do not form only through condensation, but droplets with diameters of up to 50 μm can be formed within approximately 1 h [56] if supersaturations are sustained, e.g., through lifting. Once some droplets have reached diameters between 25 and 40 μm [67,68], collision-coalescence becomes relevant [69,70]. The fall speed is proportional to the square of the droplet radius; hence, larger droplets sediment significantly faster than smaller droplets. As they descend, they collide and coalesce with smaller droplets and grow even further. Several factors influence the growth of SLDs:

1) The water vapor available in connection with the distance over which droplets are lifted (cloud depth) controls the droplet growth by diffusion in adiabatic clouds [69]. Furthermore, the cloud depth and vertical velocity within the cloud affect the distance over which a falling droplet can grow through collision-coalescence.

2) The number of CCNs determines among how many droplets the available water is shared. A large ratio of available water vapor to CCNs leads to faster diffusional growth and larger droplets.

3) Mixing processes can affect droplet size distributions in many ways; they can cause evaporation as well as diffusional growth of droplets and can also increase the chance of collision-coalescence events [67,69,71].

4) Processes like secondary ice production (SIP) [58,72], ice particles falling into the cloud from higher layers (“seeding”), and increased production of ice crystals within the clouds, often via cloud top cooling, can lead to the partial or complete depletion of supercooled liquid water, including SLDs, from the cloud [73–75].

The instrumentation aboard the SENS4ICE aircraft was insufficient to study mixing processes and ice formation or multiplication processes. As mentioned in Sec. II, the cloud depths during SENS4ICE are uncertain. We therefore investigate only the first process, the number of available CCNs. We acknowledge that other processes may have played a role, but we cannot quantify their influence.

The number concentration of CCNs is closely related to the droplet number concentration [76–78], which is therefore used as a proxy for the number concentration of CCNs. The CCN concentration depends strongly on the environment, e.g., whether the air masses are of maritime or continental origin and whether they were influenced by pollution or not. For example, typical boundary-layer clouds have cloud droplet number concentrations from 50 to about

500 cm^{-3} [79] in maritime environments and from 100 cm^{-3} to more than 1000 cm^{-3} in typical continental environments [80–82]. Most of the clouds sampled in SENS4ICE cannot be described as boundary-layer clouds. We aimed to sample clouds with few CCNs and therefore often sought cloud decks that were separated from the ground by an inversion layer. This explains the relatively low number concentrations for the continental clouds sampled during the North American campaign (see Fig. 9a). The midlevel clouds sampled during the European flight campaign had very low number concentrations that fall even well below typical values for marine clouds (Fig. 9b) and represent some of the lowest number concentrations observed in clouds containing SLDs [17,23,83].

To understand the influence of air mass origin on the measurements during the two campaigns, we separated clouds formed in continental air masses and clouds formed in maritime air masses. For all flights, the origin of the clouds was verified with NOAA's HYSPLIT trajectory model [84,85]. All clouds measured in North America formed in continental air masses, in agreement with the previous observations from the region [86]. Figure 13 shows the number concentration and the MVDs for all of the icing conditions in the North American campaign, 19% of which were Appendix O conditions. For 94% of the measurements, the number concentrations were greater than 25 cm^{-3}, for 77% they were greater than 90 cm^{-3} and for 26% they were even greater than 330 cm^{-3}. The MVDs were for 72% of the measurements smaller than 20 μm and for 97.5% smaller than 40 μm.

For the clouds measured in the European campaign, the air masses had continental origin during flights OF1, OF2.1, OF2.2, OF6, OF7, and OF8 and maritime origin for the remaining flights. Maritime air masses originated from the Atlantic; hence, they were relatively clean. The distinction between air of maritime origin and air of continental origin is to some extent uncertain, as it is unknown how quickly mixing with different air masses occurred. However, the air masses considered as maritime had traveled at most 6 h over land, mostly at altitudes well above 3000 m. The air masses classified as continental, on the other hand, had traveled at least 20 h over land, in most cases even 48 h. Figure 14 shows the percentage of Appendix O conditions measured during the European campaign in clouds with continental and maritime air masses (panels a and b, respectively) and the number concentrations and MVDs in continental and maritime clouds (panels c and d).

Panels a and b of Fig. 14 demonstrate that during the European campaign, Appendix O conditions were much more common in maritime clouds. Panel c shows that, as would be expected, number concentrations in maritime clouds were on average much lower than in continental clouds. For maritime conditions, number concentrations exceeded 25 cm^{-3} in only 16% of the measurements, compared to 80% in continental air. MVDs only exceeded 40 μm for 1.5% of the time in continental clouds, compared to 25% of the time in maritime clouds (panel d). MVDs in maritime clouds were even larger than 60 μm for 4.5% of the time.

The bimodal DSDs that we observed in the American campaign (see Fig. 8a) are strong evidence that only some drops acted as collector drops and attained large sizes. Therefore, these measurements suggest typical growth of SLDs by collision-coalescence.

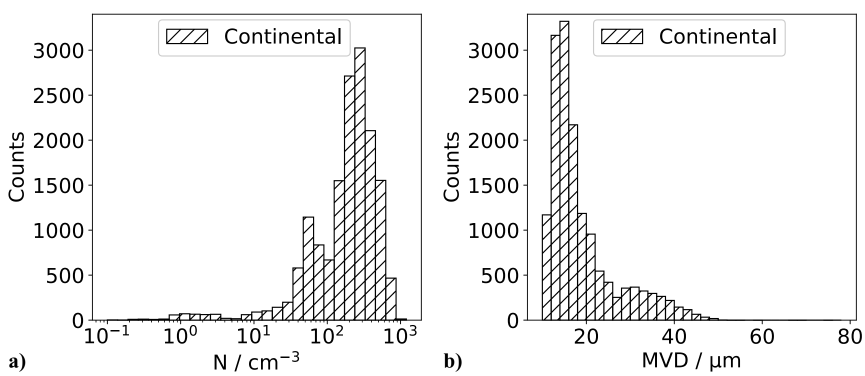

Fig. 13 Number concentrations (a) and MVDs (b) of icing conditions in North America. All clouds were of continental origin. Nineteen percent of icing conditions were Appendix O, and the remainder were Appendix C.

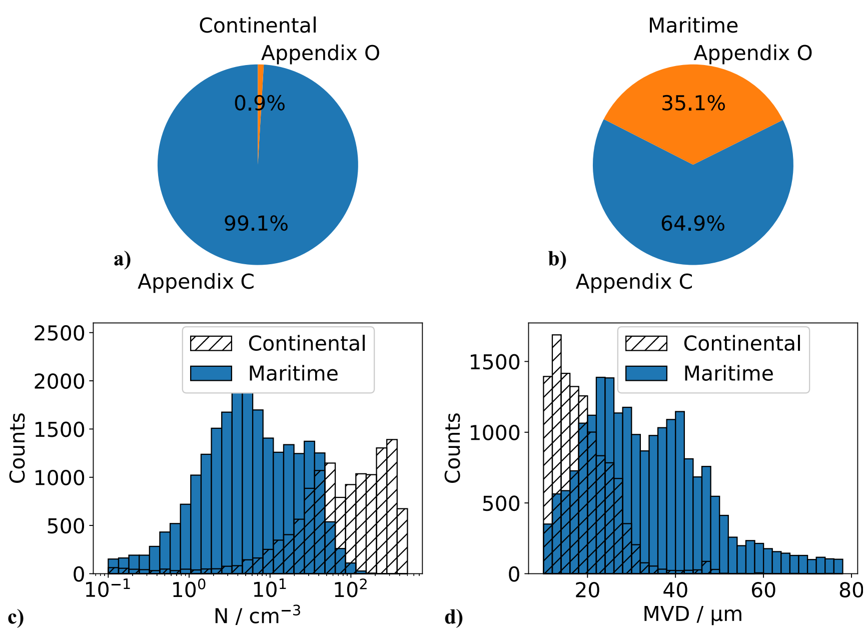

Fig. 14 Fraction of Appendix O conditions in clouds formed in continental (a) and maritime (b) air masses in Europe. The number concentrations and MVDs of the continental and maritime environments (of all icing conditions) are shown in panels (c) and (d).

In the European campaign, sampling was most often done near the cloud top, but droplet sizes in the maritime clouds were significantly larger than in the North American campaign. It is unlikely that the droplets attained their large sizes by collision-coalescence during descent through an extensive cloud. Instead, it seems that the low number of CCNs associated with maritime air masses led to the available water vapor being distributed on just a few droplets, which consequently grew to large droplet sizes by condensation. These already relatively large droplets then formed SLDs through just a few collision-coalescence events. The number of CCNs may have been further reduced by precipitation due to lift experienced by the air masses before the sampling [17,75].

We can conclude that the differences in the cumulative mass distributions of Appendix O conditions in the North American and the European campaigns are likely a consequence of the air mass origin. Low CCN concentrations in clean, maritime clouds caused DSDs with large MVDs, while higher concentrations of CCNs (compared to the maritime clouds, not in comparison to general boundary-layer clouds) in continental clouds limited the growth of the droplets, and comparatively few SLDs formed after undergoing a prolonged collision-coalescence process. This conclusion is also in line with observations from other flight campaigns, such as those presented in Williams et al. [68] and Isaac et al. [87]. However, it is important to remember that we could not investigate other factors such as cloud depth and mixing, which may also have promoted the growth of SLDs.

C. Observations of Mixed-Phase Conditions

Section V.C showed that mixed-phase conditions were rarely sampled during the North American campaign, while they were frequently encountered during the European campaign. Furthermore, the number concentration of ice particles in the mixed-phase conditions of the European campaign was relatively high compared to the overall number concentration. The SENS4ICE research aircraft did not carry instruments to study cloud processes, such as ice nucleating particle (INP) and CCN counters, or instruments to measure updraft speeds. Therefore, we can only speculate about the processes responsible for the frequent occurrence of mixed-phase clouds and the large number of ice crystals in Europe.

The absence of mixed-phase conditions during the North American campaign may be due to the measurement strategy, which targeted clouds with few ice crystals to increase the chance of finding SLDs. Hence, this paper cannot make a statement on the presence of mixed-phase conditions in the Great Lakes region in the winter months. The flight strategy of the European campaign also targeted purely supercooled clouds but often encountered mixed-phase conditions. Therefore, it can be stated that mixed-phase conditions were frequent in the springtime clouds around Toulouse.

How can the frequent occurrence of mixed-phase conditions during the European campaign be explained? Ice crystals can form on INPs [88,89]. Similar to CCNs, INPs are usually carried into the cloud from sources on the ground or the sea. For -10 and $-30°C$, typical INP concentrations are between 0.01 and 40 dm^{-3} and between 0.01 and 400 dm^{-3}, respectively [88], while typical CCN concentrations fall between 10^5 and 10^6 dm^{-3} [57,62]. Furthermore, the formation of ice particles on INP is a stochastic process, and the average nucleation time is strongly dependent on the ambient temperature [90].

Ice crystal number concentrations from the European campaign are in agreement with the INP concentrations stated by Khvorostyanov and Curry [57], but the droplet number concentration is significantly below typical CCN concentrations. Since many of the measurements of the European campaign were conducted in frontal clouds, it is possible that the number of CCNs was reduced through precipitation that occurred during lifting processes. If this was the case, the number of INPs was likely also reduced through washout. The observed number concentration of ice particles during the European campaign could then not be explained with INPs anymore. Likely, other processes were also involved. Secondary ice production [91] is a candidate, and droplet sizes between 40 and 60 μm have been found to splinter upon freezing and thus be conducive to secondary ice production [92]. During all flights of the European campaign where high ice crystal concentrations were observed, high clouds were present above the sampled midlevel clouds. Instead of initially forming on INPs, the formation of ice crystals may have been seeded with ice crystals from the clouds above. Secondary ice production may then have multiplied the ice crystal number concentrations even further.

We cannot definitively say what the main cause for the high number of mixed-phase conditions and the high number concentrations of ice crystals during the European campaign was. The theory that seeding and secondary ice production played major roles appears plausible, but more detailed studies with a larger suite of instrumentation that includes, e.g., measurements of the updraft speed and radars for the analysis of the cloud structure, would need to be performed to understand the formation of these mixed-phase clouds.

D. Encounters That Exceed the Appendix O Certification Envelopes

Section V.D showed that some SLD encounters exceeded the Appendix O certification envelopes. But what are the implications of that? The envelopes represent 99% probability limits. Naturally, some encounters will exceed them. Furthermore, the 99% limits are themselves associated with a 95% confidence interval [7]. This 95% confidence interval extends from about 0.4 to 0.53 for FZDZ MVD < 40 μm [7]. The fact that a few encounters exceeded the envelope, therefore, is consistent with previous findings.

The severity of ice accretion depends not only on LWC but also on the LWC contained in droplets of a given size. The relevant sizes in turn depend on the aircraft, its ice protection systems, and flight and atmospheric parameters, such as airspeed, angle of attack, pressure, and temperature. The underlying question is which droplet sizes lead to ice accretion on unprotected surfaces. Are 80 μm droplets already a hazard? Or only droplets exceeding 200 μm? The relevant droplet sizes may even be subject to temporal changes. Once initial ice accretion has formed, the created disturbance may allow small and large drops to further build the ice accretion. If we simplistically assume that for a certain combination of flight and atmospheric parameters, all drops larger than 100 μm impinge on unprotected surfaces of an aircraft, the LWC contained in SLD (LWC_{SLD}) and the exposure distance are relevant properties for the safety of flight. These are plotted against each other in Fig. 15. Also shown are isolines of the mass of SLDs that would accrete on one square meter of unprotected surface oriented perpendicular to the airflow (we assume that only SLDs accrete on the unprotected surfaces and that the freezing fraction is equal to 1). According to this grouping, the two most severe icing encounters are those that lie close to the 1000 $g\,m^{-2}$ isoline. These encounters are not the same as those that exceeded the envelopes. This illustrates that the most adverse icing condition depends not only on the presence of SLDs but also on the LWC in SLD conditions. For comparison, the LWC_{SLD} of the average FZDZ distribution with MVD > 40 μm from the Appendix O regulations [8] (and based on the work of Cober and Isaac [4]) is plotted under the assumption that the maximum LWC according to the certification

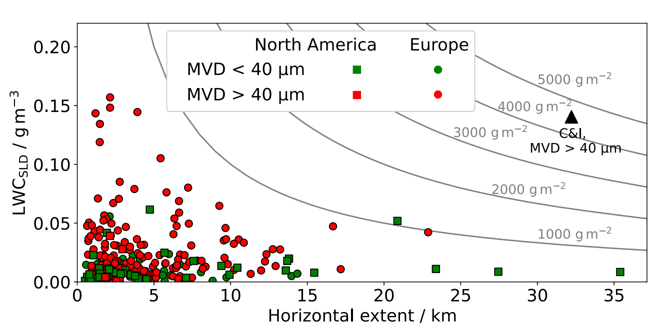

Fig. 15 Horizontal extent and LWC_{SLD} of the Appendix O encounters from North America (green) and Europe (red). Isolines of SLD ice mass accreted per square meter of unprotected cross-sectional area are plotted in light gray. The black triangle marks the LWC_{SLD} of an encounter over 17.4 nautical miles with the average distribution of FZDZ with MVD > 40 μm [8].

envelopes was encountered. The LWC_{SLD} for that scenario is much greater than any value encountered during the SENS4ICE campaigns, meaning that the fact that some encounters lie outside the envelopes does not represent a critical issue.

E. Implications on Detection of Appendix O Conditions

Future aircraft have the following options to show compliance with Appendix O [9]:

1) The aircraft can be certified for all icing conditions specified within Appendix O.

2) The aircraft can be certified for a portion of Appendix O, being required to safely exit all icing conditions once Appendix O conditions outside its certification specification are detected.

3) The aircraft can be certified to be able to detect Appendix O conditions and to subsequently fly safely while it exits all icing conditions.

As shown in Fig. 12, many Appendix O encounters, especially from the European campaign, were less than one minute long, and, according to Fig. 15, the accreted ice mass from SLDs during such a short encounter is small compared to the maximum values foreseen in the certification regulations [9]. Short encounters are problematic because their LWC does not pose a danger to the aircraft, but the presence of Appendix O conditions may require the aircraft to divert if the length of the encounter is not known a priori [93]. Therefore, especially for aircraft certified using options two and three from the list above, information is required on where the icing and Appendix O conditions are located, how their severity will evolve, and also which regions are free of icing conditions. Several tools that diagnose the presence of icing conditions, the type of icing, and the severity have been developed and are currently used operationally. These tools usually base their diagnosis on the following data sources: numerical weather prediction (NWP), satellite data, radar data, PIREPs, and surface observations. Examples for such tools are ADWICE [94,95], SIGMA [96], and CIP [97].

Icing conditions often change within a few kilometers [98]. The use of higher-resolution NWP models, such as Meteo France's AROME model with a resolution of just 1.3 km [99] or the U.S. American HRRR [100,101] with a resolution of 3 km, can bring further advancements in the prediction of local icing conditions. Additionally, two-moment cloud schemes [102–106] can yield improved predictions of drop size and could potentially provide valuable information for the prediction of SLD conditions. Furthermore, the use of polarized radar measurements from the American NEXRAD system to predict the type of hydrometeor [107,108] is currently being investigated to distinguish different categories of liquid and frozen particles.

Regions where the detection of icing conditions is challenging nonetheless remain. For example, icing conditions are difficult to detect when they are obscured from satellite view by higher clouds or when they occur close to the solar terminator, where the satellite images are difficult to interpret [109]. Radar data, on the other hand, is complicated to analyze when mixed-phase conditions are present, as the ice crystals in these conditions tend to obscure the signal from droplets. A detailed description of the existing challenges that complicate a precise forecast of icing conditions can be found in [109]. At present, the TAIWIN project [93] investigates solutions to the described challenges.

The importance of tools that predict encounter length and severity shall be stressed here. Requiring aircraft to detect and exit Appendix O conditions without the availability of such tools may lead to unnecessary reroutings and consequently higher fuel and operating costs. In the worst case, it may even lead to older aircraft types (that do not detect Appendix O) being preferred by airlines because these aircraft types are less restricted in their operation.

F. Implications for Flight Safety

In recent years, several instances of rapid ice accretion causing stalls have been documented [18,20,21,110]. Although recovery from these stalls was possible, these events emphasize the ongoing risk posed by sudden ice accretion, which pilots may not immediately recognize as hazardous or of which, as discussed in the section above, the spatial extent is unknown. Table 4 lists some of these events. The first event is described in detail also in Bernstein et al. [17]. The incidents listed here largely followed the same pattern: after takeoff, during the climb phase, the aircraft entered icing conditions that resulted in rapid ice accretion. Subsequently, due to the rapid ice buildup, the aircraft had difficulties climbing, resulting in it staying longer inside the icing conditions. In some events, the pilots also leveled off, realizing that the aircraft performance was insufficient to climb further, and tried to deviate out of the conditions.

All of the events were related to the passage of weather fronts, and the cloud layer or multiple cloud layers extended over at least 4000 ft. The short times that were spent in icing conditions until the upsets occurred are remarkable. In the most extreme case, the upset happened after just 6.5 min. Therefore, high water contents with respect to the certification envelope were likely present. Unfortunately, no information on the droplet size during these events is available, though in all cases icing on the side windows of the ATR aircraft was reported, which is usually associated with larger droplet sizes.

These events underline the need for improved tools that inform pilots and flight controllers about the position and severity of icing conditions (as discussed in Sec. VI.E). Accurate information on the icing conditions would probably have prevented these incidents. It is therefore recommended to invest further research into this topic.

VII. Conclusions

This work presented an overview of the macro- and microphysical parameters of icing conditions encountered during the two SENS4ICE flight campaigns in North America and Europe. We developed an algorithm that allows us to distinguish Appendix C and Appendix O conditions based on the analysis of OAP images. The retrieval of SLDs is associated with a missed alarm rate of 1% and a false alarm rate of 18%. Based on this retrieval, we presented statistics on the microphysical properties of Appendix C and Appendix O during the two campaigns. The wintertime icing conditions sampled during the North American campaign were mostly found in thick stratus clouds with altitudes between 1000 and 3000 m. This data adds to an already large dataset [68,107,109,111] of icing measurements in the Great Lakes regions. The early flights of the European SENS4ICE campaign sampled icing conditions at similar altitudes, but later flights predominantly sampled icing conditions in midlevel clouds. There were substantial differences between the Appendix O encounters of the North American campaign and the European campaign. Appendix O encounters during the North American campaign tended to have number concentrations between 20 and 300 cm^{-3} and an average LWC of 0.31 $g\,m^{-3}$. MVDs were often between 20 and 30 μm and the average cumulative mass distributions matched that from the Appendix O regulations [4] for FZDZ MVD < 40 μm closely. Appendix O conditions in the European campaign tended to have much lower particle number concentrations, often below 10 cm^{-3} with an average LWC around 0.14 $g\,m^{-3}$. MVDs were in many cases larger than 40 μm and the

Table 4 In-flight icing events over Europe that led to a temporary loss of control (the list shows only examples and is not exhaustive)

Aircraft	Date and time of takeoff	Route	Flight phase	Time in icing conditions before upset, min	Extent of icing conditions
ATR 42-320, LN-FAO	14 Sept. 2005, 7:20 CEST	Sørstokken– Oslo	Climb	6.5	FL100–FL140
ATR 72-212A, OY-JZC	14 Nov. 2016, 08:10 CET	Bergen– Ålesund	Horizontal	16	FL100–FL160
ATR 72-212A, G-COBO	21 Dec. 2016, 17:20 GMT	Guernsey– Manchester	Climb	9	FL090–FL130
ATR 72-212A, EC-KKQ	9 Sept. 2017, 20:10 CEST	Alicante–Madrid	Climb	8.5	FL130–FL170

droplet size distributions were in many cases close to unimodal. This work showed that one likely reason for the differences between the clouds sampled in North America and Europe was the origin of the air masses. Clouds in air masses of continental origin in Europe had similar number concentrations and MVDs to those sampled during the North American campaign. The clouds with low number concentrations and high MVDs were always found in air masses with maritime origin.

We also investigated the hazard posed by the icing conditions encountered during the two campaigns. Even though some LWCs exceeded those specified in the certification envelopes of Appendix O, from the combination of droplet size distribution, encounter length, and LWC, we determined that none of the encounters was more severe than the most intense FZDZ case foreseen in the certification specifications.

Appendix A: Comparison of the LWCs of the CDPs of DLR and SAFIRE

Two different CDPs, one of DLR and the other owned by SAFIRE, were aboard the SAFIRE ATR 42. Only the CDP of DLR was used in the evaluation. A comparison of the LWC measured by the two probes is shown in Fig. A1. A least-square fit to the data shows that the CDP of SAFIRE measured on average a 9% higher LWC than the CDP of DLR, with the R^2 of the fit being 0.904. A value of 9% is well within the uncertainty range that is assumed for scattering probes [112].

Appendix B: Comparison of LWCs and TWCs Measured by Hotwire Instruments During the European Campaign

Three hotwire instruments are used in the data evaluation of the European campaign. The LWC300 for the measurement of the LWC, and the Robust probe and the Nevzorov probe for the measurement of the TWC. A comparison of the results of the instruments can be seen in Fig. B1.

Figure B1a compares the measurements of the LWC300 and the TWC measured by the 8 mm cone of the Nevzorov probe; the MVD measured by the CDP is shown in color code. Only measurements where $N_{LAS} < 1000\ m^{-3}$ were considered for the analysis to exclude mixed-phase segments where the LWC is not equal to the TWC. The least-square fit shows that the LWC300 measurement is on average 26% lower than that of the 8 mm cone of the Nevzorov probe. The R^2 is 0.705. An analysis of the data showed that LWCs from the two instruments corresponded within 15% when the MVD from the CDP was larger than 20 μm and smaller than 40 μm. For smaller and larger MVDs of the CDP, the LWC300 measured less than 85% of the LWC of the Nevzorov probe. The lower measurements of the LWC300 for larger MVDs are expected because large droplets splash on the cylindrical sensor and are only partially collected. No clear reason for the measurement of lower LWCs by the LWC300 for small MVDs of the CDP was found.

Figure B1b shows a comparison between the Nevzorov 8 mm TWC cone and the TWC measured by the Robust probe. Results from the least-square fit show that the Robust probe measurement is on average only 69% of that of the 8 mm TWC cone of the Nevzorov probe. The R^2 is 0.837. The color code shows the number of large ice crystals. The Robust probe especially measures lower TWC compared to the Nevzorov probe when many large ice crystals are present. If segments with $N_{LAS} \geq 1000\ m^{-3}$ are excluded from the analysis, the Robust probe measures 80% of the TWC of the Nevzorov probe and R^2 improves to 0.86 (not shown). The sensor of the Robust probe is not as deep as that of the Nevzorov probe. The Nevzorov 8 mm TWC cone might therefore be more efficient at collecting ice crystals, which would be in agreement with the observations described in Lilie et al. [32].

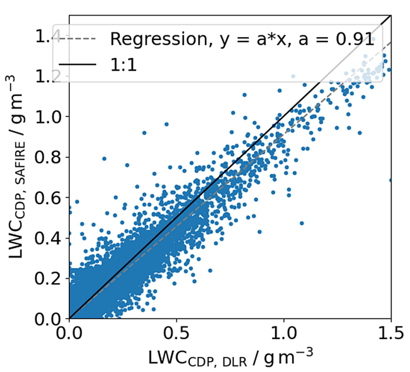

Fig. A1 Comparison of the LWCs measured by the CDP of DLR and the CDP of SAFIRE.

Acknowledgments

This project has received funding from the European Union's Horizon 2020 research and innovation program under grant agreement N° 82425 (SENS4ICE). Further funding was provided by the Deutsche Forschungsgemeinschaft (TRR 301, Project-ID 428312742) and (SPP1294, VO1504/10-1, Project ID 522359172). The North American SENS4ICE flight campaign was financed by Embraer. Airborne data for the European SENS4ICE flight campaign was obtained using the aircraft managed by SAFIRE, the French facility for airborne research, an infrastructure of the French National Center for Scientific Research (CNRS), Météo-France, and the French National Center for Space Studies (CNES). We express our appreciation to the SENS4ICE project management team, including Carsten Schwarz, Christoph Deiler, and Falk Sachs. We are also thankful to Lyle Lilie and Dan Bouley for their support with the measurement equipment during the

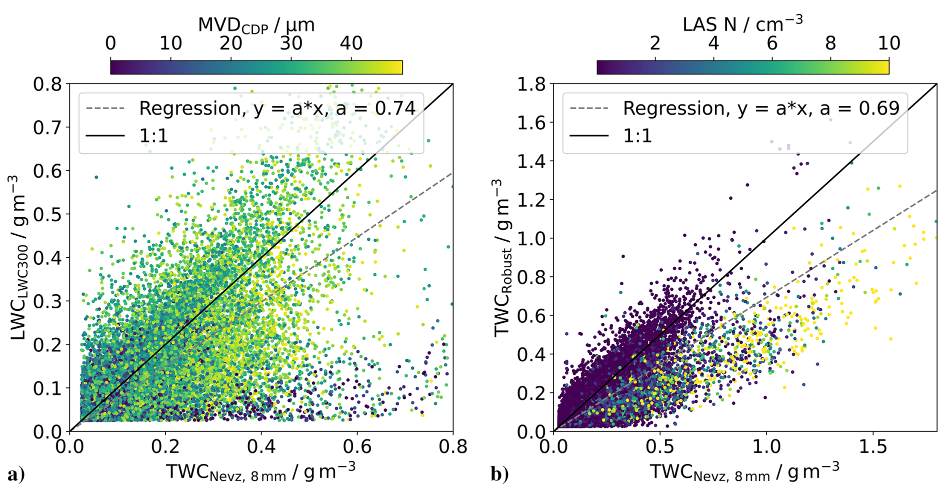

Fig. B1 Comparison of LWC measurements from the LWC300 sensor and the Nevzorov 8 mm TWC cone (a) and of the TWC from the Robust probe and the Nevzorov 8 mm TWC cone (b).

North American campaign, as well as Daniel Martins da Silva and the Embraer team for facilitating the campaign. The European campaign greatly benefited from the support of weather forecasters from Météo France and the German weather service (DWD), as well as the hard work and flexibility of the SAFIRE and DLR teams. We gratefully acknowledge the NOAA Air Resources Laboratory (ARL) for the provision of the HYSPLIT transport and dispersion model and/ READY website (https://www.ready.noaa.gov) used in this publication. Artificial intelligence was used to check grammar and spelling and for the formatting of figures and tables.

References

[1] Sand, W. R., Cooper, W. A., Politovich, M. K., and Veal, D. L., "Icing Conditions Encountered by a Research Aircraft," *Journal of Climate and Applied Meteorology*, Vol. 23, No. 10, 1984, pp. 1427–1440. https://doi.org/10.1175/0733-3021-23.10.1427

[2] Cooper, W. A., Sand, W. R., Veal, D. L., and Politovich, M. K., "Effects of Icing on Performance of a Research Airplane," *Journal of Aircraft*, Vol. 21, No. 9, 1984, pp. 708–715. https://doi.org/10.2514/3.45018

[3] Politovich, M. K., "Aircraft Icing Caused by Large Supercooled Droplets," *Journal of Applied Meteorology and Climatology*, Vol. 28, No. 9, 1989, pp. 856–868. https://doi.org/10.1175/1520-0450(1989)028<0856:AICBLS>2.0.CO;2

[4] Cober, S. G., and Isaac, G. A., "Characterization of Aircraft Icing Environments with Supercooled Large Drops for Application to Commercial Aircraft Certification," *Journal of Applied Meteorology and Climatology*, Vol. 51, No. 2, 2012, pp. 265–284. https://doi.org/10.1175/JAMC-D-11-022.1

[5] National Transportation Safety Board, "In-Flight Icing Encounter and Loss of Control Simmons Airlines, d.b.a. American Eagle Flight 4184 Avions de Transport Regional (ATR) Model 72-212, N401AM Roselawn, Indiana October 31, 1994," TR. NTSB/AAR-96/01, National Transportation Safety Board, 1994.

[6] Marwitz, J., Politovich, M., Bernstein, B., Ralph, F., Neiman, P., Ashenden, R., and Bresch, J., "Meteorological Conditions Associated with the ATR72 Aircraft Accident Near Roselawn, Indiana, on 31 October 1994," *Bulletin of the American Meteorological Society*, Vol. 78, No. 1, 1997, pp. 41–52. https://doi.org/10.1175/1520-0477(1997)078<0041:MCAWTA>2.0.CO;2

[7] Cober, S., Bernstein, B., Jeck, R., Hill, E., Isaac, G., Riley, J., and Shah, A., "Data and Analysis for the Development of an Engineering Standard for Supercooled Large Drop Conditions," TR DOT/FAA/AR-09/10, Federal Aviation Administration, 2009.

[8] Office of the Federal Register, National Archives and Records Administration, "14 CFR Appendix O to Part 25 - Supercooled Large Drop Icing Conditions," Jan. 2016, https://www.govinfo.gov/app/details/CFR-2016-title14-vol1/CFR-2016-title14-vol1-part25-appO.

[9] European Aviation Safety Agency (EASA), "Certification Specifications and Acceptable Means of Compliance for Large Aeroplanes," 2021, https://www.easa.europa.eu/downloads/134259/en.

[10] Schwarz, C. W., "The SENS4ICE EU project - SENSors and certifiable hybrid architectures for safer aviation in ICing Environment - A project midterm overview," *6th International Conference Prospects of Civil Avionics Development*, International Council of the Aeronautical Sciences Paper 2022_0794, 2021, https://elib.dlr.de/144361/.

[11] Schwarz, C., "SENS4ICE EU Project Preliminary Results," *SAE Technical Paper Series*, SAE International Paper 2023-01-1496, 2023. https://doi.org/10.4271/2023-01-1496

[12] Deiler, C., Schwarz, C., Ridouane, E. H., Orazzo, A., and Jurkat-Witschas, T., "Final Report on Evaluation of Technologies Developed in SENS4ICE and Technical Project Results," 2024. https://doi.org/10.5281/ZENODO.11520452

[13] Ridouane, E. H., "Sensor Evaluation Results and Final Roadmaps for Future Technology Development and Exploitation," 2024. https://doi.org/10.5281/ZENODO.11520165

[14] Deiler, C., and Sachs, F., "Design and Testing of an Indirect Ice Detection Methodology," *SAE Technical Paper Series*, SAE International Paper 2023-01-1493, 2023. https://doi.org/10.4271/2023-01-1493

[15] Orazzo, A., Thillays, B., and Deiler, C., "Final Report on Hybrid Ice Detection Development," 2024. https://doi.org/10.5281/ZENODO.11520284

[16] Lucke, J., Zollo, A., Jurkat-Witschas, T., and Bernstein, B., "Final Report on Airborne Demonstration and Atmospheric Characterisation," 2024. https://doi.org/10.5281/ZENODO.11520416

[17] Bernstein, B. C., Rasmussen, R. M., McDonough, F., and Wolff, C., "Keys to Differentiating Between Small- and Large-Drop Icing Conditions in Continental Clouds," *Journal of Applied Meteorology and Climatology*, Vol. 58, No. 9, 2019, pp. 1931–1953. https://doi.org/10.1175/JAMC-D-18-0038.1

[18] Authority, Norwegian Safety Investigation, "Report on Serious Aviation Incident West of Forde Airport Bringeland on 14 November 2016 Involving ATR72-212A, OY-JZC, Operated by Jet Time AS," TR, Norwegian Safety Investigation Authority, 2020.

[19] Green, S. D., "The Icemaster Database and an Analysis of Aircraft Aerodynamic Icing Accidents and Incidents," TR, Federal Aviation Administration, 2015.

[20] Air Accidents Investigation Branch, "AAIB Bulletin 12/2017," TR, Air Accidents Investigation Branch, 2017.

[21] Civil Aviation Accident and Incident Investigation Commission, "Incident Involving an ATR 72-212A Aircraft, Registration EC-KKQ, Operated by Swiftair, at Flight Level 170 in the Vicinity of Reporting Point NARGO (Albacete-Spain) on 9 September 2017," Civil Aviation Accident and Incident Investigation Commission, 2017.

[22] Cober, S. G., Isaac, G. A., Korolev, A. V., and Strapp, J. W., "Assessing Cloud-Phase Conditions," *Journal of Applied Meteorology*, Vol. 40, No. 11, 2001, pp. 1967–1983. https://doi.org/10.1175/1520-0450(2001)040<1967:ACPC>2.0.CO;2

[23] Rosenfeld, D., Chemke, R., DeMott, P., Sullivan, R. C., Rasmussen, R., McDonough, F., Comstock, J., Schmid, B., Tomlinson, J., Jonsson, H., et al., "The Common Occurrence of Highly Supercooled Drizzle and Rain Near the Coastal Regions of the Western United States," *Journal of Geophysical Research: Atmospheres*, Vol. 118, No. 17, 2013, pp. 9819–9833. https://doi.org/10.1002/jgrd.50529

[24] Isaac, G., Cober, S., Korolev, A., Strapp, J., Tremblay, A., and Marcotte, D., "Overview of the Canadian Freezing Drizzle Experiment I, II, and III," *Conference on Cloud Physics*, American Meteorological Soc. Paper FRL-1998-0027, 1998, pp. 447–450.

[25] Miller, D., Bernstein, B., McDonough, B., and Strapp, J., "NASA/FAA/NCAR Supercooled Large Droplet Icing Flight Research—Summary of Winter 96–97 Flight Operations," *36th AIAA Aerospace Sciences Meeting and Exhibit*, AIAA Paper 1998-577, 1998. https://doi.org/10.2514/6.1998-577

[26] Bernstein, B. C., Wolff, C. A., and McDonough, F., "An Inferred Climatology of Icing Conditions Aloft, Including Supercooled Large Drops. Part I: Canada and the Continental United States," *Journal of Applied Meteorology and Climatology*, Vol. 46, No. 11, 2007, pp. 1857–1878. https://doi.org/10.1175/2007JAMC1607.1

[27] Hauf, T., and Schröder, F., "Aircraft Icing Research Flights in Embedded Convection," *Meteorology and Atmospheric Physics*, Vol. 91, Nos. 1–4, 2005, pp. 247–265. https://doi.org/10.1007/s00703-004-0082-y

[28] Fernández-González, S., Sánchez, J. L., Gascón, E., López, L., García-Ortega, E., and Merino, A., "Weather Features Associated with Aircraft Icing Conditions: A Case Study," *Scientific World Journal*, Vol. 2014, 2014, pp. 1–18. https://doi.org/10.1155/2014/279063

[29] Bolgiani, P., Fernández-González, S., Martin, M. L., Valero, F., Merino, A., García-Ortega, E., and Sánchez, J. L., "Analysis and Numerical Simulation of an Aircraft Icing Episode Near Adolfo Suárez Madrid-Barajas International Airport," *Atmospheric Research*, Vol. 200, 2018, pp. 60–69. https://doi.org/10.1016/j.atmosres.2017.10.001

[30] Bernstein, B., "Meteorological Analysis of Selected Natural Icing Flights—SENS4ICE North America Campaign," TR, Leading Edge Atmospherics, LLC, 2023.

[31] SAFIRE, "safire.fr," 2024, [retrieved 23 May 2023].

[32] Lilie, L. E., Bouley, D., Sivo, C. P., and Ratvasky, T. P., "Test Results for the SEA Ice Crystal Detector (ICD) Under SLD Conditions at the NASA IRT," AIAA Paper 2021-2654, 2021. https://doi.org/10.2514/6.2021-2654

[33] Esposito, B. M., Orchard, D., Lucke, J., Nichman, L., Bliankinshtein, N., Lilie, L., Catalano, P., D'Aniello, F., and Strapp, J. W., "Comparability of Hot-Wire Estimates of Liquid Water Content in SLD Conditions," *SAE Technical Paper Series*, SAE International Paper 2023-01-1423, 2023. https://doi.org/10.4271/2023-01-1423

[34] Lance, S., Brock, C. A., Rogers, D., and Gordon, J. A., "Water Droplet Calibration of the Cloud Droplet Probe (CDP) and in-Flight Performance in Liquid, Ice and Mixed-Phase Clouds During ARCPAC," *Atmospheric Measurement Techniques*, Vol. 3, No. 6, 2010, pp. 1683–1706. https://doi.org/10.5194/amt-3-1683-2010

[35] Faber, S., French, J. R., and Jackson, R., "Laboratory and in-Flight Evaluation of Measurement Uncertainties from a Commercial Cloud Droplet Probe (CDP)," *Atmospheric Measurement Techniques*, Vol. 11, No. 6, 2018, pp. 3645–3659. https://doi.org/10.5194/amt-11-3645-2018

[36] De La Torre Castro, E., Jurkat-Witschas, T., Afchine, A., Grewe, V., Hahn, V., Kirschler, S., Krämer, M., Lucke, J., Spelten, N., Wernli, H., et al., "Differences in Microphysical Properties of Cirrus at High and Mid-Latitudes," *Atmospheric Chemistry and Physics*, Vol. 23, No. 20, 2023, pp. 13,167–13,189. https://doi.org/10.5194/acp-23-13167-2023

[37] Knollenberg, R. G., "The Optical Array: An Alternative to Scattering or Extinction for Airborne Particle Size Determination," *Journal of Applied Meteorology (1962-1982)*, Vol. 9, No. 1, 1970, pp. 86–103.

[38] Korolev, A. V., Strapp, J. W., and Isaac, G. A., "Evaluation of the Accuracy of PMS Optical Array Probes," *Journal of Atmospheric and Oceanic Technology*, Vol. 15, No. 3, 1998, pp. 708–720. https://doi.org/10.1175/1520-0426(1998)015<0708:EOTAOP>2.0.CO;2

[39] Jurkat-Witschas, T., Lucke, J., Schwarz, C., Deiler, C., Sachs, F., Kirschler, S., Menekay, D., Voigt, C., Bernstein, B., Jaron, O., et al., "Overview of Cloud Microphysical Measurements during the SENS4ICE Airborne Test Campaigns," *SAE Technical Paper Series*, SAE International Paper 2023-01-1491, 2023. https://doi.org/10.4271/2023-01-1491

[40] Bony, S., Lothon, M., Delanoë, J., Coutris, P., Etienne, J.-C., Aemisegger, F., Albright, A. L., André, T., Bellec, H., Baron, A., et al., "EUREC4A Observations from the SAFIRE ATR42 Aircraft," *Earth System Science Data*, Vol. 14, No. 4, 2022, pp. 2021–2064. https://doi.org/10.5194/essd-14-2021-2022

[41] Braga, R. C., Rosenfeld, D., Weigel, R., Jurkat, T., Andreae, M. O., Wendisch, M., Pöschl, U., Voigt, C., Mahnke, C., Borrmann, S., et al., "Further Evidence for CCN Aerosol Concentrations Determining the Height of Warm Rain and Ice Initiation in Convective Clouds over the Amazon Basin," *Atmospheric Chemistry and Physics*, Vol. 17, No. 23, 2017, pp. 14,433–14,456. https://doi.org/10.5194/acp-17-14433-2017

[42] Moser, M., Voigt, C., Jurkat-Witschas, T., Hahn, V., Mioche, G., Jourdan, O., Dupuy, R., Gourbeyre, C., Schwarzenboeck, A., Lucke, J., et al., "Microphysical and Thermodynamic Phase Analyses of Arctic Low-Level Clouds Measured Above the Sea Ice and the Open Ocean in Spring and Summer," *Atmospheric Chemistry and Physics*, Vol. 23, No. 13, 2023, pp. 7257–7280. https://doi.org/10.5194/acp-23-7257-2023

[43] King, W. D., Parkin, D. A., and Handsworth, R. J., "A Hot-Wire Liquid Water Device Having Fully Calculable Response Characteristics," *Journal of Applied Meteorology and Climatology*, Vol. 17, No. 12, 1978, pp. 1809–1813. https://doi.org/10.1175/1520-0450(1978)017<1809:AHWLWD>2.0.CO;2

[44] Droplet Measurement Technologies, "LWC-300/301 Liquid Water Content Sensor Operator's Manual," DOC-0361, 2018.

[45] Rigby, D. L., and Struk, P. M., "Simulation of Fluid Flow and Collection Efficiency at Low Stokes Number," *AIAA Aviation 2020 Forum*, AIAA Paper 2020-2811, 2020. https://doi.org/10.2514/6.2020-2811

[46] Science Engineering Associates, "WCM-3000 Operating Manual," 2024.

[47] Korolev, A. V., Strapp, J. W., Isaac, G. A., and Nevzorov, A. N., "The Nevzorov Airborne Hot-Wire LWC–TWC Probe: Principle of Operation and Performance Characteristics," *Journal of Atmospheric and Oceanic Technology*, Vol. 15, No. 6, 1998, pp. 1495–1510. https://doi.org/10.1175/1520-0426(1998)015<1495:TNAHWL>2.0.CO;2

[48] Strapp, J. W., Lilie, L. E., Ratvasky, T. P., Davison, C. R., and Dumont, C., "Isokinetic TWC Evaporator Probe: Development of the IKP2 and Performance Testing for the HAIC-HIWC Darwin 2014 and Cayenne Field Campaigns," *8th AIAA Atmospheric and Space Environments Conference*, AIAA Paper 2016-4059, 2016.

[49] Lucke, J., Jurkat-Witschas, T., Heller, R., Hahn, V., Hamman, M., Breitfuss, W., Bora, V. R., Moser, M., and Voigt, C., "Icing Wind Tunnel Measurements of Supercooled Large Droplets Using the 12 mm Total Water Content Cone of the Nevzorov Probe," *Atmospheric Measurement Techniques*, Vol. 15, No. 24, 2022, pp. 7375–7394. https://doi.org/10.5194/amt-15-7375-2022

[50] Billault-Roux, A.-C., Grazioli, J., Delanoë, J., Jorquera, S., Pauwels, N., Viltard, N., Martini, A., Mariage, V., Le Gac, C., Caudoux, C., et al., "ICE GENESIS: Synergetic Aircraft and Ground-Based Remote Sensing and In Situ Measurements of Snowfall Microphysical Properties," *Bulletin of the American Meteorological Society*, Vol. 104, No. 2, 2023, pp. E367–E388. https://doi.org/10.1175/BAMS-D-21-0184.1

[51] Esposito, B. M., Bachalo, W. D., Leroy, D., Schwarzenboeck, A., Jurkat, T., Voigt, C., and Bansmer, S., "Wind Tunnel Measurements of Simulated Glaciated Cloud Conditions to Evaluate Newly Developed 2D Imaging Probes," *SAE Technical Paper Series*, SAE International Paper 2019-01-1981, 2019. https://doi.org/10.4271/2019-01-1981

[52] Lucke, J., "Detection and Differentiation of Supercooled Large Drop Icing Conditions," Ph.D. Thesis, Delft Univ. of Technology, The Netherlands, 2024, pp. 111–113.

[53] Schwarzenboeck, A., Mioche, G., Armetta, A., Herber, A., and Gayet, J.-F., "Response of the Nevzorov Hot Wire Probe in Clouds Dominated by Droplet Conditions in the Drizzle Size Range," *Atmospheric Measurement Techniques*, Vol. 2, No. 2, 2009, pp. 779–788. https://doi.org/10.5194/amt-2-779-2009

[54] Korolev, A., Strapp, J., Isaac, G., and Emery, E., "Improved Airborne Hot-Wire Measurements of Ice Water Content in Clouds," *Journal of Atmospheric and Oceanic Technology*, Vol. 30, No. 9, 2013, pp. 2121–2131. https://doi.org/10.1175/JTECH-D-13-00007.1

[55] Korolev, A., and Strapp, J., "Accuracy of Measurements of Cloud Ice Water Content by the Nevzorov Probe," *40th AIAA Aerospace Sciences Meeting & Exhibit*, AIAA Paper 2002-679, 2002. https://doi.org/10.2514/6.2002-679

[56] Pruppacher, H., and Klett, J., *Microphysics of Clouds and Precipitation*, Springer-Verlag, Berlin, 2010. https://doi.org/10.1007/978-0-306-48100-0

[57] Khvorostyanov, V. I., and Curry, J. A., "The Theory of Ice Nucleation by Heterogeneous Freezing of Deliquescent Mixed CCN. Part I: Critical Radius, Energy, and Nucleation Rate," *Journal of the Atmospheric Sciences*, Vol. 61, No. 22, 2004, pp. 2676–2691. https://doi.org/10.1175/JAS3266.1

[58] Korolev, A., DeMott, P. J., Heckman, I., Wolde, M., Williams, E., Smalley, D. J., and Donovan, M. F., "Observation of Secondary Ice Production in Clouds at Low Temperatures," *Atmospheric Chemistry and Physics*, Vol. 22, No. 19, 2022, pp. 13,103–13,113. https://doi.org/10.5194/acp-22-13103-2022

[59] Pasquier, J. T., Henneberger, J., Ramelli, F., Lauber, A., David, R. O., Wieder, J., Carlsen, T., Gierens, R., Maturilli, M., and Lohmann, U., "Conditions Favorable for Secondary Ice Production in Arctic Mixed-Phase Clouds," *Atmospheric Chemistry and Physics*, Vol. 22, No. 23, 2022, pp. 15,579–15,601. https://doi.org/10.5194/acp-22-15579-2022

[60] Wu, W., and McFarquhar, G. M., "On the Impacts of Different Definitions of Maximum Dimension for Nonspherical Particles Recorded by 2D Imaging Probes," *Journal of Atmospheric and Oceanic Technology*, Vol. 33, No. 5, 2016, pp. 1057–1072. https://doi.org/10.1175/JTECH-D-15-0177.1

[61] Korolev, A., "Reconstruction of the Sizes of Spherical Particles from Their Shadow Images. Part I: Theoretical Considerations," *Journal of Atmospheric and Oceanic Technology*, Vol. 24, No. 3, 2007, pp. 376–389. https://doi.org/10.1175/JTECH1980.1

[62] Kirschler, S., "Effekte von Aerosol und Dynamik auf die Eigenschaften ozeanischer Wolken im Nordwestatlantik," Ph.D. Thesis, Johannes Gutenberg-Universität in Mainz, Mainz, Germany, 2023.

[63] Menekay, D., "Comparative Analysis of Optical in-Situ Probes and the MSG Satellite for Improved Detection of Aircraft Icing Conditions," Master's Thesis, Technische Universität München, München, Germany, 2023, p. 40, https://elib.dlr.de/201912/.

[64] de Guélis, T. V., Schwarzenböck, A., Shcherbakov, V., Gourbeyre, C., Laurent, B., Dupuy, R., Coutris, P., and Duroure, C., "Study of the Diffraction Pattern of Cloud Particles and the Respective Responses of Optical Array Probes," *Atmospheric Measurement Techniques*, Vol. 12, No. 4, 2019, pp. 2513–2529. https://doi.org/10.5194/amt-12-2513-2019

[65] Lilie, L., Bouley, D., Sivo, C., Esposito, B., Bansemer, A., Heller, R., and Strapp, J. W., "A New 1D2D Optical Array Particle Imaging Probe for Airborne and Ground Simulation Cloud Measurements," SAE TP 2023-01-1415, 2023.

[66] Korolev, A., McFarquhar, G., Field, P. R., Franklin, C., Lawson, P., Wang, Z., Williams, E., Abel, S. J., Axisa, D., Borrmann, S., et al., "Mixed-Phase Clouds: Progress and Challenges," *Meteorological Monographs*, Vol. 58, 2017, pp. 5.1–5.50. https://doi.org/10.1175/AMSMONOGRAPHS-D-17-0001.1

[67] Korolev, A. V., and Isaac, G. A., "Drop Growth due to High Supersaturation Caused by Isobaric Mixing," *Journal of the Atmospheric Sciences*, Vol. 57, No. 10, 2000, pp. 1675–1685. https://doi.org/10.1175/1520-0469(2000)057<1675:DGDTHS>2.0.CO;2

[68] Williams, E., Donovan, M., Smalley, D., Kurdzo, J., and Bennett, B., "The 2017 Buffalo Area Icing and Radar Study (BAIRS II)," MIT Lincoln Lab. TR ATC-447, 2020.

[69] Freud, E., and Rosenfeld, D., "Linear Relation Between Convective Cloud Drop Number Concentration and Depth for Rain Initiation," *Journal of Geophysical Research: Atmospheres*, Vol. 117, No. D2, 2012. https://doi.org/10.1029/2011JD016457

[70] Rosenfeld, D., Zheng, Y., Hashimshoni, E., Pöhlker, M. L., Jefferson, A., Pöhlker, C., Yu, X., Zhu, Y., Liu, G., Yue, Z., et al., "Satellite Retrieval of Cloud Condensation Nuclei Concentrations by Using Clouds as CCN Chambers," *National Academy of Sciences of the United States of America*, Vol. 113, No. 21, 2016, pp. 5828–5834. https://doi.org/10.1073/pnas.1514044113

[71] Korolev, A., Khain, A., Pinsky, M., and French, J., "Theoretical Study of Mixing in Liquid Clouds—Part 1: Classical Concepts," *Atmospheric Chemistry and Physics*, Vol. 16, No. 14, 2016, pp. 9235–9254. https://doi.org/10.5194/acp-16-9235-2016

[72] Hallett, J., and Mossop, S. C., "Production of Secondary Ice Particles During the Riming Process," *Nature*, Vol. 249, No. 5452, 1974, pp. 26–28. https://doi.org/10.1038/249026a0

[73] Boatman, J. F., and Reinking, R. F., "Synoptic and Mesoscale Circulations and Precipitation Mechanisms in Shallow Upslope Storms over the Western High Plains," *Monthly Weather Review*, Vol. 112, No. 9, 1984, pp. 1725–1744. https://doi.org/10.1175/1520-0493(1984)112<1725:SAMCAP>2.0.CO;2

[74] Politovich, M. K., and Bernstein, B. C., "Production and Depletion of Supercooled Liquid Water in a Colorado Winter Storm," *Journal of Applied Meteorology and Climatology*, Vol. 34, No. 12, 1995, pp. 2631–2648. https://doi.org/10.1175/1520-0450(1995)034<2631:PADOSL>2.0.CO;2

[75] Rasmussen, R. M., Bernstein, B. C., Murakami, M., Stossmeister, G., Reisner, J., and Stankov, B., "The 1990 Valentine's Day Arctic Outbreak. Part I: Mesoscale and Microscale Structure and Evolution of a Colorado Front Range Shallow Upslope Cloud," *Journal of Applied Meteorology*, Vol. 34, No. 7, 1995, pp. 1481–1511. https://doi.org/10.1175/1520-0450-34.7.1481

[76] Twomey, S., "The Nuclei of Natural Cloud Formation Part II: The Supersaturation in Natural Clouds and the Variation of Cloud Droplet Concentration," *Geofisica Pura e Applicata*, Vol. 43, No. 1, 1959, pp. 243–249. https://doi.org/10.1007/BF01993560

[77] Hudson, J. G., and Yum, S. S., "Maritime-Continental Drizzle Contrasts in Small Cumuli," *Journal of the Atmospheric Sciences*, Vol. 58, No. 8, 2001, pp. 915–926. https://doi.org/10.1175/1520-0469(2001)058<0915:MCDCIS>2.0.CO;2

[78] Yum, S. S., and Hudson, J. G., "Maritime/Continental Microphysical Contrasts in Stratus," *Tellus B: Chemical and Physical Meteorology*, Vol. 54, No. 1, 2002, p. 61. https://doi.org/10.3402/tellusb.v54i1.16648

[79] Twomey, S., *Introduction to the Mathematics of Inversion in Remote Sensing and Indirect Measurement*. 3rd ed., Elsevier Scientific Publ., Amsterdam, 1977, p. 253.

[80] McCoy, D. T., Bender, F. A.-M., Grosvenor, D. P., Mohrmann, J. K., Hartmann, D. L., Wood, R., and Field, P. R., "Predicting Decadal Trends in Cloud Droplet Number Concentration Using Reanalysis and Satellite Data," *Atmospheric Chemistry and Physics*, Vol. 18, No. 3, 2018, pp. 2035–2047. https://doi.org/10.5194/acp-18-2035-2018

[81] Chubb, T., Huang, Y., Jensen, J., Campos, T., Siems, S., and Manton, M., "Observations of High Droplet Number Concentrations in Southern Ocean Boundary Layer Clouds," *Atmospheric Chemistry and Physics*, Vol. 16, No. 2, 2016, pp. 971–987. https://doi.org/10.5194/acp-16-971-2016

[82] Kirschler, S., Voigt, C., Anderson, B. E., Chen, G., Crosbie, E. C., Ferrare, R. A., Hahn, V., Hair, J. W., Kaufmann, S., Moore, R. H., et al., "Overview and Statistical Analysis of Boundary Layer Clouds and Precipitation over the Western North Atlantic Ocean," *Atmospheric Chemistry and Physics*, Vol. 23, No. 18, 2023, pp. 10,731–10,750. https://doi.org/10.5194/acp-23-10731-2023

[83] Lasher-Trapp, S., Anderson-Bereznicki, S., Shackelford, A., Twohy, C. H., and Hudson, J. G., "An Investigation of the Influence of Droplet Number Concentration and Giant Aerosol Particles Upon Supercooled Large Drop Formation in Wintertime Stratiform Clouds," *Journal of Applied Meteorology and Climatology*, Vol. 47, No. 10, 2008, pp. 2659–2678. https://doi.org/10.1175/2008JAMC1807.1

[84] Stein, A. F., Draxler, R. R., Rolph, G. D., Stunder, B. J. B., Cohen, M. D., and Ngan, F., "NOAA's HYSPLIT Atmospheric Transport and Dispersion Modeling System," *Bulletin of the American Meteorological Society*, Vol. 96, No. 12, 2015, pp. 2059–2077. https://doi.org/10.1175/BAMS-D-14-00110.1

[85] Rolph, G., Stein, A., and Stunder, B., "Real-Time Environmental Applications and Display sYstem: READY," *Environmental Modelling & Software*, Vol. 95, 2017, pp. 210–228. https://doi.org/10.1016/j.envsoft.2017.06.025

[86] Bernstein, B. C., Mcdonough, F., and Wolff, C., "A Regional Comparison of Icing Conditions in Boundary Layer Clouds," *SAE Technical Paper Series*, SAE International Paper 2011-38-0021, 2011. https://doi.org/10.4271/2011-38-0021

[87] Isaac, G., Cober, S., Strapp, J., Korolev, A., Tremblay, A., and Marcotte, D., "Recent Canadian Research on Aircraft in-Flight Icing," *Canadian Aeronautics and Space Journal*, Vol. 47, No. 3, 2001, pp. 213–221.

[88] DeMott, P. J., Prenni, A. J., Liu, X., Kreidenweis, S. M., Petters, M. D., Twohy, C. H., Richardson, M. S., Eidhammer, T., and Rogers, D. C., "Predicting Global Atmospheric Ice Nuclei Distributions and Their Impacts on Climate," *National Academy of Sciences of the United States of America*, Vol. 107, No. 25, 2010, pp. 11,217–11,222. https://doi.org/10.1073/pnas.0910818107

[89] Kreidenweis, S. M., Petters, M., and Lohmann, U., "100 Years of Progress in Cloud Physics, Aerosols, and Aerosol Chemistry Research," *Meteorological Monographs*, Vol. 59, 2019, pp. 11.1–11.72. https://doi.org/10.1175/AMSMONOGRAPHS-D-18-0024.1

[90] Vonnegut, B., and Baldwin, M., "Repeated Nucleation of a Supercooled Water Sample that Contains Silver Iodide Particles," *Journal of Applied Meteorology and Climatology*, Vol. 23, No. 3, 1984, pp. 486–490. https://doi.org/10.1175/1520-0450(1984)023<0486:RNOASW>2.0.CO;2

[91] Field, P. R., Lawson, R. P., Brown, P. R. A., Lloyd, G., Westbrook, C., Moisseev, D., Miltenberger, A., Nenes, A., Blyth, A., Choularton, T., et al., "Chapter 7. Secondary Ice Production: Current State of the Science and Recommendations for the Future," *Meteorological Monographs*, Vol. 58, 2016, p. 7-1. https://doi.org/10.1175/AMSMONOGRAPHS-D-16-0014.1

[92] Korolev, A., Heckman, I., Wolde, M., Ackerman, A. S., Fridlind, A. M., Ladino, L. A., Lawson, R. P., Milbrandt, J., and Williams, E., "A New Look at the Environmental Conditions Favorable to Secondary Ice Production," *Atmospheric Chemistry and Physics*, Vol. 20, No. 3, 2020, pp. 1391–1429. https://doi.org/10.5194/acp-20-1391-2020

[93] DiVito, S., Landolt, S., Berstein, B., Green, S., Bracken, J., Wolde, M., Nichman, L., Alvidrez, S., and Maciejewski, C., "Latest Developments in Terminal Area Icing by the FAA Terminal Area Icing Weather Information for NextGen (TAIWIN) Project," *SAE International Conference on Icing of Aircraft, Engines, and Structures*, SAE International, 2023.

[94] Tafferner, A., Hauf, T., Leifeld, C., Hafner, T., Leykauf, H., and Voigt, U., "ADWICE: Advanced Diagnosis and Warning System for Aircraft Icing Environments," *Weather and Forecasting*, Vol. 18, No. 2, 2003, pp. 184–203. https://doi.org/10.1175/1520-0434(2003)018<0184:AADAWS>2.0.CO;2

[95] Kalinka, F., Roloff, K., Tendel, J., and Hauf, T., "The In-Flight Icing Warning System ADWICE for European Airspace—Current Structure, Recent Improvements and Verification Results," *Meteorologische Zeitschrift*, Vol. 26, No. 4, 2017, pp. 441–455. https://doi.org/10.1127/metz/2017/0756

[96] Le Bot, C., "SIGMA: System of Icing Geographic identification in Meteorology for Aviation," *SAE TP Series*, SAE International Paper 2023-01-2085, 2003. https://doi.org/10.4271/2003-01-2085

[97] Bernstein, B. C., McDonough, F., Politovich, M. K., Brown, B. G., Ratvasky, T. P., Miller, D. R., Wolff, C. A., and Cunning, G., "Current

Icing Potential: Algorithm Description and Comparison with Aircraft Observations," *Journal of Applied Meteorology*, Vol. 44, No. 7, 2005, pp. 969–986.
https://doi.org/10.1175/JAM2246.1

[98] Faber, S., Bernstein, B., Landolt, S., Jacobson, D., DiVito, S., Wolde, M., Korolev, A., Heckman, I., Nichman, L., and Nguyen, C., "Airborne Observations of Highly Variable and Complex Freezing Drizzle and Mixed-Phase Environments," *Journal of Applied Meteorology and Climatology*, Vol. 63, No. 11, 2024, pp. 1343–1361.
https://doi.org/10.1175/JAMC-D-24-0056.1

[99] Seity, Y., Brousseau, P., Malardel, S., Hello, G., Bénard, P., Bouttier, F., Lac, C., and Masson, V., "The AROME-France Convective-Scale Operational Model," *Monthly Weather Review*, Vol. 139, No. 3, 2011, pp. 976–991.
https://doi.org/10.1175/2010MWR3425.1

[100] Benjamin, S. G., Weygandt, S. S., Brown, J. M., Hu, M., Alexander, C. R., Smirnova, T. G., Olson, J. B., James, E. P., Dowell, D. C., Grell, G. A., et al., "A North American Hourly Assimilation and Model Forecast Cycle: The Rapid Refresh," *Monthly Weather Review*, Vol. 144, No. 4, 2016, pp. 1669–1694.
https://doi.org/10.1175/MWR-D-15-0242.1

[101] Benjamin, S. G., Brown, J. M., and Smirnova, T. G., "Explicit Precipitation-Type Diagnosis from a Model Using a Mixed-Phase Bulk Cloud-Precipitation Microphysics Parameterization," *Weather and Forecasting*, Vol. 31, No. 2, 2016, pp. 609–619.
https://doi.org/10.1175/WAF-D-15-0136.1

[102] Meyers, M. P., Walko, R. L., Harrington, J. Y., and Cotton, W. R., "New RAMS Cloud Microphysics Parameterization. Part II: The Two-Moment Scheme," *Atmospheric Research*, Vol. 45, No. 1, 1997, pp. 3–39.
https://doi.org/10.1016/S0169-8095(97)00018-5

[103] Thompson, G., and Eidhammer, T., "A Study of Aerosol Impacts on Clouds and Precipitation Development in a Large Winter Cyclone," *Journal of the Atmospheric Sciences*, Vol. 71, No. 10, 2014, pp. 3636–3658.
https://doi.org/10.1175/JAS-D-13-0305.1

[104] Vié, B., Pinty, J.-P., Berthet, S., and Leriche, M., "LIMA (v1.0): A Quasi Two-Moment Microphysical Scheme Driven by a Multimodal Population of Cloud Condensation and Ice Freezing Nuclei," *Geoscientific Model Development*, Vol. 9, No. 2, 2016, pp. 567–586.
https://doi.org/10.5194/gmd-9-567-2016

[105] Muench, S., and Lohmann, U., "Developing a Cloud Scheme With Prognostic Cloud Fraction and Two Moment Microphysics for ECHAM-HAM," *Journal of Advances in Modeling Earth Systems*, Vol. 12, No. 8, 2020, Paper e2019MS001824.
https://doi.org/10.1029/2019MS001824

[106] Field, P. R., Hill, A., Shipway, B., Furtado, K., Wilkinson, J., Miltenberger, A., Gordon, H., Grosvenor, D. P., Stevens, R., and Van Weverberg, K., "Implementation of a Double Moment Cloud Microphysics Scheme in the UK Met Office Regional Numerical Weather Prediction Model," *Quarterly Journal of the Royal Meteorological Society*, Vol. 149, No. 752, 2023, pp. 703–739.
https://doi.org/10.1002/qj.4414

[107] Williams, E., Donovan, M., Smalley, D., Hallowell, R., Griffin, E., Hood, K., and Bennett, B., "The 2013 Buffalo Area Icing and Radar Study (BAIRS)," MIT Lincoln Lab. TR ATC-419, 2015.

[108] Serke, D. J., Ellis, S. M., Tessendorf, S. A., Albo, D. E., Hubbert, J. C., and Haggerty, J. A., "Radar Icing Algorithm: Algorithm Description and Comparison with Aircraft Observations," *Journal of Atmospheric and Oceanic Technology*, Vol. 39, No. 1, 2022, pp. 91–109.
https://doi.org/10.1175/JTECH-D-21-0003.1

[109] Bernstein, B., DiVito, S., Riley, J. T., Landolt, S., Haggerty, J., Thompson, G., Adriaansen, D., Serke, D., Kessinger, C., Tessendorf, S., et al., "The In-Cloud Icing and Large-Drop Experiment Science and Operations Plan," TR DOT/FAA/TC-21/29, Dept. of Transportation, Federal Aviation Administration, William J. Hughes Technical Center, 2021.
https://doi.org/10.21949/1524472

[110] Norway, A. I. B., "Report on the Serious Incident over Glacier Folgefonna, Norway on 14 September 2005 with ATR 42-320, LN-FAO, Operated by Coast Air AS," TR, Accident Investigation Board Norway, 2009.

[111] Cober, S. G., Isaac, G. A., and Strapp, J. W., "Characterizations of Aircraft Icing Environments that Include Supercooled Large Drops," *Journal of Applied Meteorology and Climatology*, Vol. 40, No. 11, 2001, pp. 1984–2002.
https://doi.org/10.1175/1520-0450(2001)040<1984:COAIET>2.0.CO;2

[112] Baumgardner, D., Abel, S. J., Axisa, D., Cotton, R., Crosier, J., Field, P., Gurganus, C., Heymsfield, A., Korolev, A., Krämer, M., et al., "Cloud Ice Properties: In Situ Measurement Challenges," *Meteorological Monographs*, Vol. 58, 2017, pp. 9.1–9.23.
https://doi.org/10.1175/AMSMONOGRAPHS-D-16-0011.1

J. Kuchar
Associate Editor